11-3-2023

A multi-organ maize metabolic model connects temperature stress with energy production and reducing power generation

Niaz Bahar Chowdhury

Margaret Simons- Senftle

Berengere Decouard

Isabelle Quillere

Martine Rigault

See next page for additional authors

Authors

Niaz Bahar Chowdhury, Margaret Simons- Senftle, Berengere Decouard, Isabelle Quillere, Martine Rigault, Karuna Anna Sajeevan, Bibek Acharya, Ratul Chowdhury, Bertrand Hirel, Alia Dellagi, Costas Maranas, and Rajib Saha

iScience

CellPress
OPEN ACCESS

Article

A multi-organ maize metabolic model connects temperature stress with energy production and reducing power generation

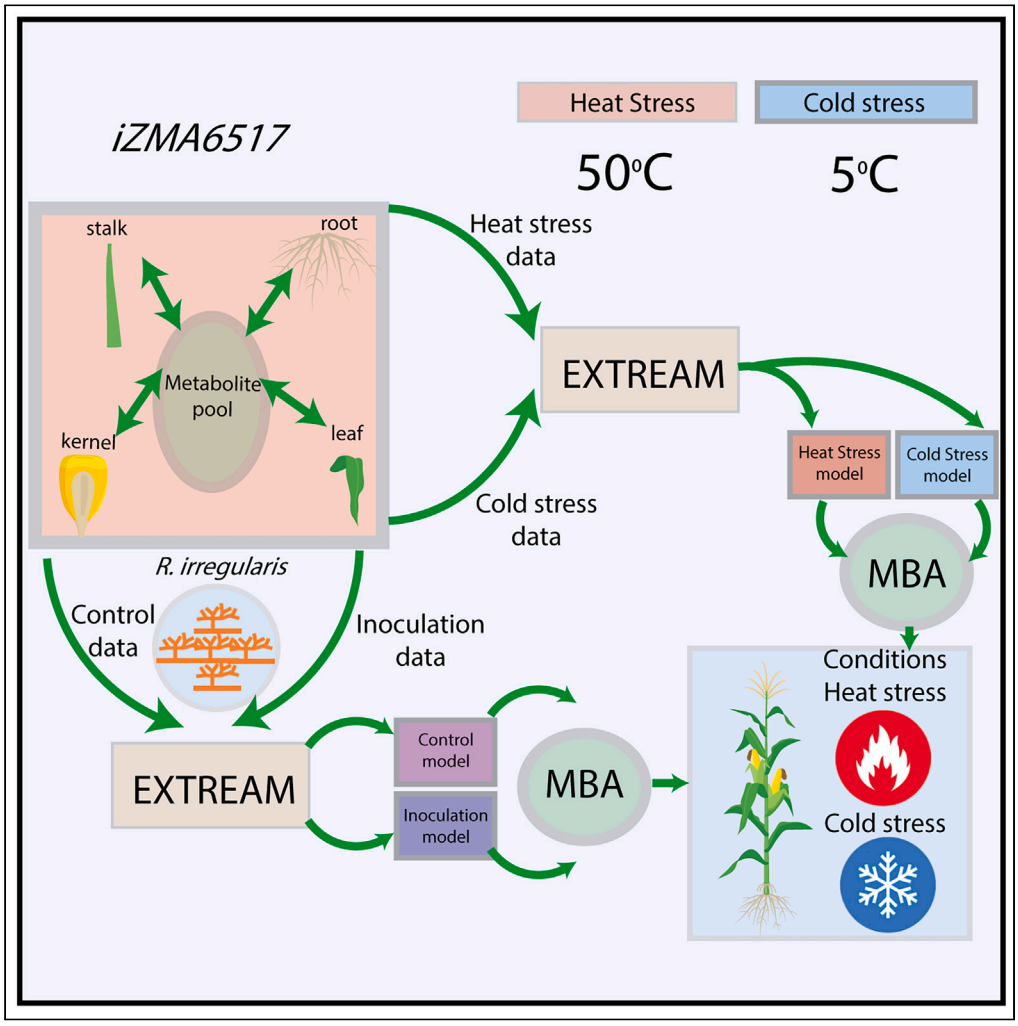

Niaz Bahar Chowdhury, Margaret Simons-Senftle, Berengere Decouard, ..., Alia Dellagi, Costas Maranas, Rajib Saha

rsaha2@unl.edu

Highlights

We reconstructed the largest maize B73 multi-organ plant metabolic model, iZMA6517

The proposed transcriptomics data integration algorithm, EXTREAM, successfully predicted the starch distribution pattern in the maize leaf

Metabolic Bottleneck Analysis (MBA) pinpointed plant-wide metabolic bottlenecks for heat and cold stresses

We demonstrated that *Rhizophagus irregularis* can effectively reduces temperature stress in maize

Chowdhury et al., iScience *26*, 108400
December 15, 2023
https://doi.org/10.1016/j.isci.2023.108400

iScience

CellPress
OPEN ACCESS

Article

A multi-organ maize metabolic model connects temperature stress with energy production and reducing power generation

Niaz Bahar Chowdhury,[1] Margaret Simons-Senftle,[2,6] Berengere Decouard,[3,6] Isabelle Quillere,[3] Martine Rigault,[3] Karuna Anna Sajeevan,[4] Bibek Acharya,[4] Ratul Chowdhury,[4] Bertrand Hirel,[5] Alia Dellagi,[3] Costas Maranas,[2] and Rajib Saha[1,7,*]

SUMMARY

Climate change has adversely affected maize productivity. Thereby, a holistic understanding of metabolic crosstalk among its organs is important to address this issue. Thus, we reconstructed the first multi-organ maize metabolic model, *i*ZMA6517, and contextualized it with heat and cold stress transcriptomics data using expression distributed reaction flux measurement (EXTREAM) algorithm. Furthermore, implementing metabolic bottleneck analysis on contextualized models revealed differences between these stresses. While both stresses had reducing power bottlenecks, heat stress had additional energy generation bottlenecks. We also performed thermodynamic driving force analysis, revealing thermodynamics-reducing power-energy generation axis dictating the nature of temperature stress responses. Thus, a temperature-tolerant maize ideotype can be engineered by leveraging the proposed thermodynamics-reducing power-energy generation axis. We experimentally inoculated maize root with a beneficial mycorrhizal fungus, *Rhizophagus irregularis*, and as a proof-of-concept demonstrated its efficacy in alleviating temperature stress. Overall, this study will guide the engineering effort of temperature stress-tolerant maize ideotypes.

INTRODUCTION

Temperature stress, resulting from global climate change, can reduce maize productivity by 7–18%.[1] Thus, there is a pressing need to develop high-yielding maize genotypes capable of withstanding temperature stress. A metabolism-centric approach can be useful to achieve that. Hence, an in-depth understanding of the impact of temperature on plant-wide metabolism is required. Such impacts include, but are not limited to, reduced photosynthesis and carbohydrate synthesis in leaves,[2] reduced starch synthesis in kernels,[3,4] upregulation of amino acid and downregulation of diterpenoid metabolism in root,[4] and lignin biosynthesis in stalks.[5] In addition to metabolism, temperature stress can directly damage enzymes and tissues,[6] impair flowering,[7] and trigger oxidative stress at the reproductive stage.[8] Additionally, the reproductive stage of the crops such as maize, tomato, soybean, rice, and cotton is susceptible to temperature stress[9] since the temperature rise at the panicle or flowering stage can reduce the fertility or inactivate the flower of the corp.[10] Although these studies were note-worthy, a holistic plant-wide understanding of temperature stress responses, delineating the interactions between vegetative and reproductive organs at key stages of plant development, is still in its infancy. Moreover, the plant-wide effect of well-known beneficial arbuscular mycorrhizal fungi (AMF), such as *Rhizophagus irregularis*,[11] has not been evaluated for its potential to alleviate temperature stress on maize growth. A multi-organ genome-scale metabolic model (GSM) is suited to address these issues. The first multi-organ plant GSM was reconstructed for barley,[12] subsequently for barrelclover,[13] arabidopsis,[14,15] soybean,[16] foxtail millet,[17] and rice.[18] These models were useful to characterize inter-organs crosstalk under various conditions. Thus, for a holistic understanding of plant-wide temperature stress responses of maize, we reconstructed the first multi-organ maize GSM, *i*ZMA6517, integrating comprehensive root, stalk, kernel, and leaf GSMs.

Contextualization of GSM by integrating "omics" data is a crucial step to connect metabolism to phenotypes. There are two classes of algorithms for contextualization: valve approaches (assuming reactions fluxes and transcript levels are proportional) and switch approaches (assuming reaction are turned on/off based on transcript levels). Earlier studies discussed the suitability of both approaches,[19] showing E-flux algorithm[20] (a valve approach) capturing better phenotypic predictions. However, E-flux algorithm can predict unrealistic phenotypes too.[21]

[1]Chemical and Biomolecular Engineering, University of Nebraska-Lincoln, Lincoln, NE, USA
[2]Chemical Engineering, The Pennsylvania State University, University Park, PA, USA
[3]Université Paris-Saclay, INRAE, AgroParisTech, Institut Jean-Pierre Bourgin (IJPB), 78000 Versailles, France
[4]Chemical and Biological Engineering, Iowa State University, Ames, IA, USA
[5]Centre de Versailles-Grignon, Institut National de Recherche pour l'Agriculture, Versailles, France
[6]These authors contributed equally
[7]Lead contact
*Correspondence: rsaha2@unl.edu
https://doi.org/10.1016/j.isci.2023.108400

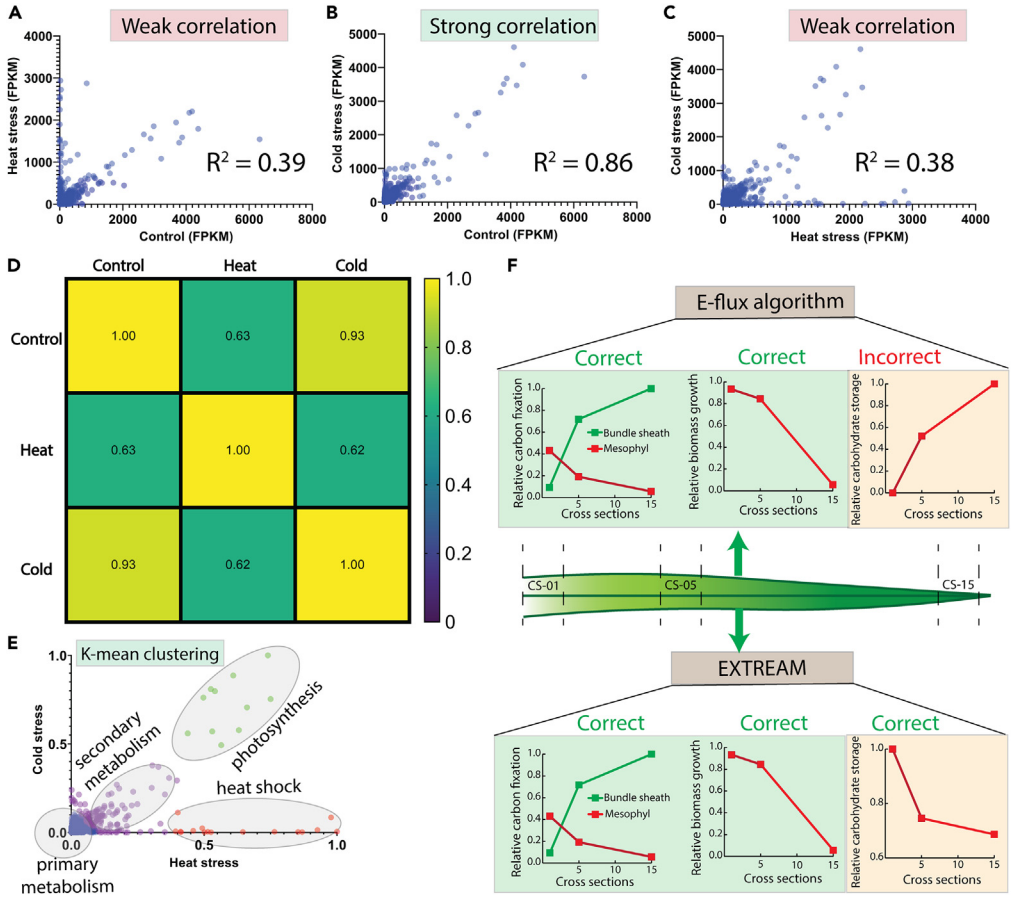

Figure 1. Transcriptomics data analysis and introduction to EXTREAM algorithm

(A) Scatterplot of control and cold stress transcriptomics data.

(B) Scatterplot of control and heat stress transcriptomics data.

(C) Scatterplot of heat and cold stresses transcriptomics data.

(D) Correlation matrix among control, heat stress, and cold stress (95% confidence interval, two-tail test).

(E) K-means clustering analysis of heat and cold stress data.

(F) E-flux and EXTREAM both predicted correct biomass production and carbon fixation for three selected cross sections of leaf, whereas only EXTREAM predicted the correct leaf starch content.

Thereby, to improve the phenotypic prediction accuracy, there is a need to develop a valve approach which can address this limitation. To achieve this, we proposed the expression distributed reaction flux measurement (EXTREAM) algorithm. Moreover, we propose a metabolic bottleneck analysis (MBA) algorithm to pinpoint metabolic bottlenecks in *i*ZMA6517.

In this study, we combined *i*ZMA6517, EXTREAM, and MBA to dissect plant-wide responses of temperature stress by pinpointing metabolic bottlenecks in different organs and to determine if responses to cold and heat share common characteristics. We found reducing power capacity had a pivotal role in responses to both stresses. Additionally, heat stress responses incurred energy generation bottlenecks. Thermodynamic driving force analysis of bottleneck pathways highlighted the role of thermodynamics-reducing power-energy generation axis when plants are subjected to temperature stress. Finally, as a proof of concept, we extended our analysis by integrating maize "omics" data when the plant is inoculated with the *R. irregularis* in *i*ZMA6517 and found that the inoculation has the potential to alleviate temperature stresses. Ultimately, this study could offer a blueprint to engineer robust abiotic stress-tolerant maize ideotypes.

RESULTS

Maize responses to heat and cold stress

To decipher maize responses to temperature stress, heat and cold-stress-related transcriptomic data of B73 genotype were collected from the literature.[22] Seedlings were subjected to cold (5^0 C for 16 h) or heat (50^0 C for 4 h) stresses, compared to a control condition (24^0 C). All plants were grown in the autoclaved soil collected from field. While heat stress drastically affected transcriptional response compared to control conditions (Figure 1A), the effect of cold stress was similar to control conditions (Figure 1B), indicating a difference of plant adaptations to

temperature stresses (Figures 1C and 1D). To explore the components of temperature stresses, we performed K-means clustering (Figure 1E) on both heat and cold stress data, identifying four distinct clusters followed by gene enrichment analyses (Figures S1–S4). These analyses revealed that photosynthesis-related genes (cluster 2) were upregulated under both stress conditions. In addition, heat shock genes (cluster 3) were upregulated in heat stress conditions. Clusters 1 and 4 revealed genes associated with central carbon and secondary metabolism, respectively.

As photosynthesis is one of the core metabolic features of plants, cluster 2 was examined in further detail. A previous study indicated a similar high transcriptional response of photosynthetic genes under temperature stress.[23] However, photosynthetic activity of plants, as measured through decreased rubisco activation,[24] decreases under temperature stress. This suggests potential metabolic bottlenecks in plant tissues preventing higher photosynthetic activity in leaves. A contextualized multi-organ GSM of maize can identify such bottlenecks. There may also be bottlenecks between transcription and translation, such as mRNA degradation, however, that would be outside of the scope of GSM. Next, we will design a suitable algorithm for such contextualization of GSM.

EXTREAM algorithm

Our previous study used the E-flux algorithm[25] to accurately predict the maize root phenotype under nitrogen starvation based on transcriptomic data. This work involved photosynthetic tissues, having additional metabolic complexities compared to roots. Thereby, the efficacy of the E-flux algorithm was re-assessed.

In a previous study, the maize leaf was divided into 15 cross-sections, and generated transcriptomics data for each of these sections.[26] For this study, we collected transcriptomics data of cross-based on the greenness of the leaf blade (less green to greener). These data were integrated in the leaf GSM[27] using E-flux algorithm. The highest growth rates in maize leaves occur at the base of the leaf, where new cells are actively dividing and elongating. As the cells grow toward the tip, they undergo expansion and maturation, leading to a decrease in the growth rate. Eventually, the cells at the tip stop elongating altogether. The contextualized leaf model correctly predicted higher biomass growth rate of leaf base compared to leaf tip (Figure 1F). The model also predicted rate of carbon fixation correctly, however, it incorrectly predicted the starch distribution profile along the leaf (Figure 1F). Thus, modification of the E-flux algorithm was required to fit the starch distribution profile.

To achieve this, we proposed the EXTREAM algorithm, which equally distributed transcript levels for each gene based on the number of cognate biochemical reactions. Once we contextualized the leaf model with the EXTREAM algorithm, it predicted the correct biomass growth rate, carbon fixation, and starch distribution profiles along the selected leaf sections (Figure 1F). Thus, EXTREAM algorithm can be effective in modeling plant organs, including photosynthetic organs.

Multi-organ genome-scale metabolic model of maize

In this study, we reconstructed the first multi-organ maize GSM, *i*ZMA6517 (Figure 2A) for the B73 genotype. The model is based on the previously reconstructed root and leaf-specific GSMs,[19,27] and newly reconstructed stalk and kernel GSMs, connected via vascular tissues (Table S1).

To further refine our existing leaf model, we identified thermodynamically infeasible cycles (TICs) and resolved those using our previously developed OptFill[28] pipeline. For stalk and kernel GSMs, we assigned gene-protein-reaction (GPR) relationships to all known reactions based on the MaizeCyc database.[29] The GPR relationships used Boolean logic to determine if enzymes associated with metabolic reactions are encoded by isozymes (OR relationship) or protein complexes (AND relationship). We next identified organ-specific reactions and the corresponding metabolic pathways by categorizing each gene's expression level for each organ. Next, we reconstructed the stalk and kernel biomass equation based on literature (Table S2). Upon completing the pathway participation in the organ-specific GSMs, we carried out gap-filling.

Finally, *i*ZMA6517 was assembled by connecting organ-specific GSMs via vascular tissues, namely phloem and xylem (Figure 2B). Although phloem and xylem are distinct tissues, the direction of the flow of metabolites was sufficient to determine if it was present in either one of those. Therefore, the two tissues were combined for simplicity. These vascular tissues will facilitate inter-organ crosstalk by translocating metabolites from one organ to another. For example, sugars travel from the leaf tissue to other tissues via the vascular tissues. Similarly, nutrients, such as nitrate and phosphate, are uptaken by root and distributed to the other organs. Table S3 has details on inter-organ transfer of metabolites. *i*ZMA6517 also improved phenotype predictions in different organs compared to the individual organ model. For example, while additional constraint was required for the individual root metabolic model to uptake water, no such constraint was required for the root model in *i*ZMA6517. Overall, *i*ZMA6517 contains 6,517 genes, 5,228 unique reactions, and 3,007 unique metabolites. Among these, 2,305 reactions (Figure 2C), 2,405 metabolites (Figure 2D), and 6,285 genes (Figure 2E) were common across all organs.

Next, to assess plant-wide impact of temperature stress, we contextualized *i*ZMA6517 for heat and cold stresses using the EXTREAM algorithm (Figure 2F). The transcriptomics data from the seedling were the aggregate data of root, stalk, and leaf. As kernel is a sink, like a previous study where it showed that there is a control of assimilates translocation from stalk to kernels,[30] we assumed the metabolism of kernel will be dictated by the aggregate behavior of root, stalk, and leaf. Thus, the aggregate transcriptomics data were used to contextualize the model (*i*ZMA6517) comprising root, stalk, kernel, and leaf under heat and cold stress. Previous studies showed control conditions had the highest nutrient uptakes, followed by heat and cold stress.[31] Once these nutrient uptakes patterns were implemented in contextualized *i*ZMA6517s, control and cold-stressed plants showed the highest and lowest biomass growth rates, respectively (both individual organs and

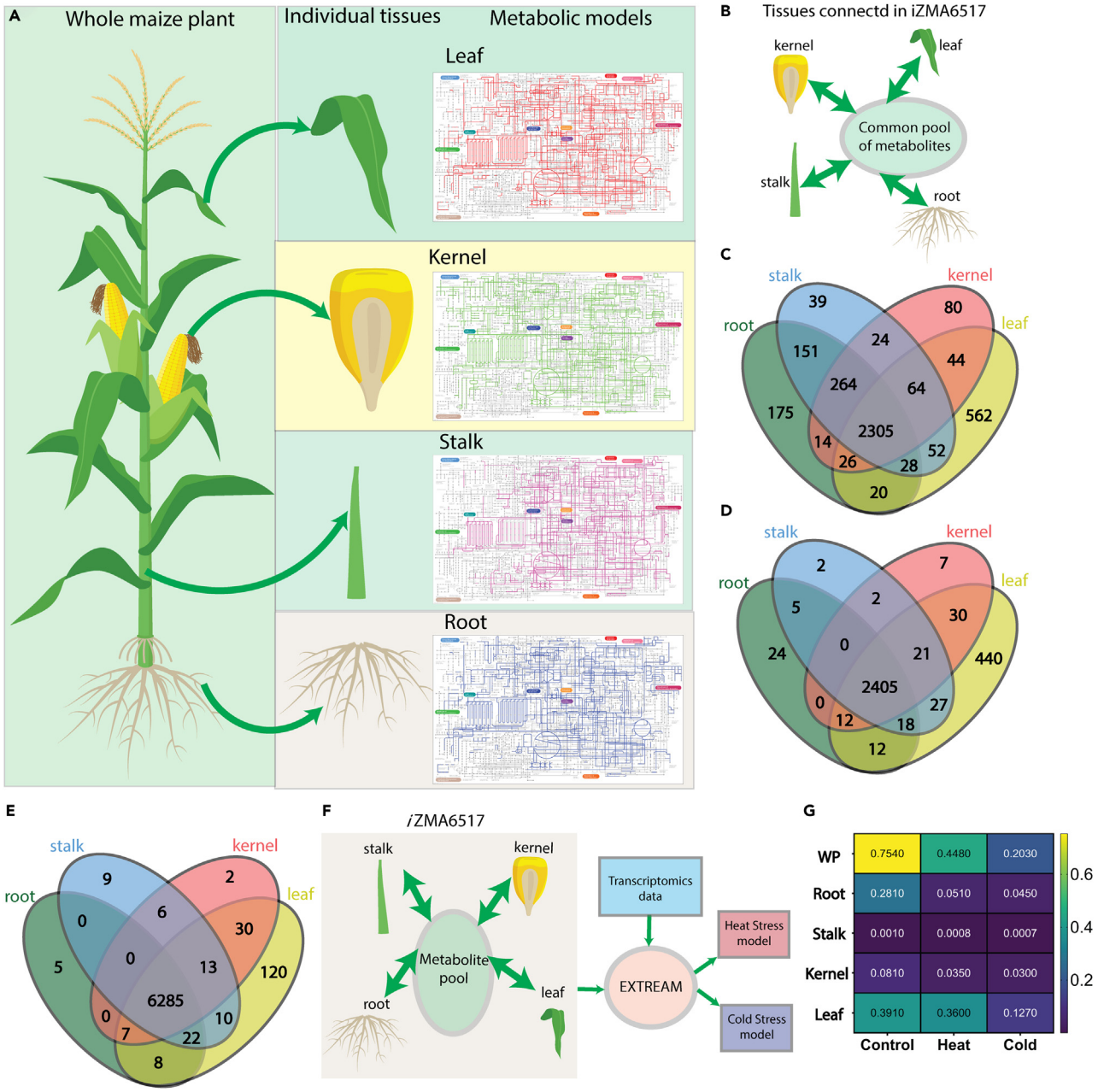

Figure 2. Overview of *i*ZMA6517 reconstruction and contextualization

(A) Individual metabolic models for root, stalk, kernel, and leaf.

(B) Connection between individual tissues via the vascular tissues.

(C) Comparison of reactions among the individual GSMs.

(D) Comparison of metabolites among the individual GSMs.

(E) Comparison of unique genes among the individual GSMs.

(F) Incorporating heat and cold stress related transcriptomics data with the iZMA6517 using the EXTREAM algorithm.

(G) EXTREAM algorithm predicted lower biomass production in each organ and in the whole plant (WP) during the cold stress compared to the heat stress.

whole plant) (Figure 2G), supporting previous studies.[32] Indeed, by projecting the aggregate transcriptomics data from seedling to kernel, we were able to predict the correct growth rate pattern for kernel in control, heat stress, and cold stress (Figure 2G). That confirms our initial assumption that, as a sink, the kernel metabolism is dictated by other organs like root, stalk, and leaf. Thus, the contextualized *i*ZMA6517 were suitable for identifying metabolic bottlenecks of temperature stresses.

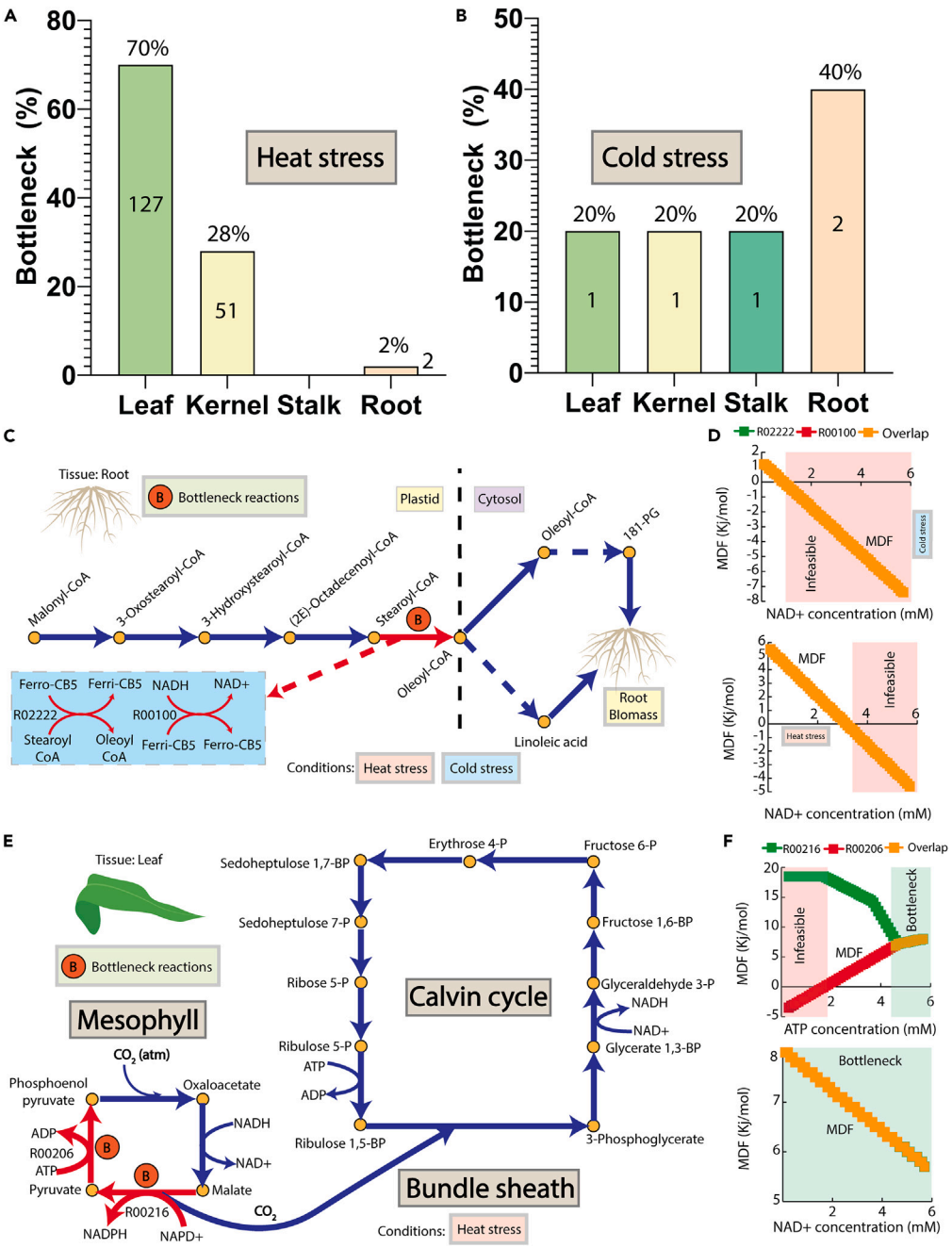

Figure 3. Identification of temperature stress bottlenecks

(A) Organ specific bottleneck reactions for heat stress (number of reactions is indicated inside the column).

(B) Organ specific bottleneck reactions for cold stress, (number of reactions is indicated inside the column).

(C) Cytochrome *b*5 reductase bottleneck in the fatty acid metabolism for heat and cold stress.

(D) Thermodynamic driving force analysis in fatty acid metabolism.

(E) Pyruvate-phosphate dikinase and malate dehydrogenase bottlenecks in the photosynthetic pathway for heat stress.

(F) Thermodynamic driving force analysis of the photosynthetic pathway.

Identification of metabolic bottlenecks

To assess the impact of temperature stress on maize metabolism, we implemented MBA to contextualized *i*ZMA6517s. MBA expanded the flux space of each reaction separately and assessed its impact on the whole plant biomass growth rate. It revealed 180 bottleneck reactions under heat stress, of which 70% occurred in leaves, 28% in kernels, and 2% in roots (Figure 3A). These reactions were distributed across

purine metabolism, pyrimidine metabolism, fatty acid metabolism, the Calvin cycle, and glycolysis (Figure S5). Among these 180 reactions, root cytochrome *b*5 reductase (24%) and acyl-ACP-hydrolase (24%) increased the plant biomass growth rate the most. Here, percentages indicate increase in biomass growth rate after debottlenecking a specific bottleneck reaction, compared to the biomass growth rate of corresponding stress condition before debottlenecking. Overall, 19 reactions increased plant biomass growth rate by more than 10% (Figure S6).

For cold stress, MBA revealed five different bottleneck reactions. Two of these occurred in the root, and one each in other organs (Figure 3B). Among those five reactions, similar to the heat stress, cytochrome *b*5 reductase in roots (182%) and leaves (147%) and acyl-ACP-hydrolase in roots (146%) increased the plant biomass growth rate the most. The stalk coniferyl-aldehyde dehydrogenase (32%) and the kernel phosphohexomutase (4%) were other bottleneck reactions.

As reaction thermodynamics is influenced by temperature, we applied Min/Max Driving Force (MDF) analysis to pathways containing bottleneck reactions, within the physiological range of substrate concentration (0.01 mM–10 mM)[33] to assess the impact of thermodynamics on those pathways. The standard Gibbs free energy of reactions was calculated (Table S4) using the group contribution method.[34] The root cytochrome *b*5 reductase and acyl-ACP-hydrolase were common to both temperature stresses. The reaction catalyzed by cytochrome *b*5 reductase is part of the fatty acid biosynthesis pathway (Figure 3C) and impacted the production of 18:1-phosphoglycerate choline and linoleic acid of biomass components. MDF analysis indicated that, with an NAD^+ concentration greater than 1.1 mM (cold stress) and 3.7 mM (heat stress), the fatty acid biosynthesis pathway was thermodynamically feasible and the cytochrome *b*5 reductase had the lowest driving force (Figure 3D). Acyl-ACP-hydrolase is involved in the fatty acid biosynthesis pathway and impacted the octadecanoic acid of biomass components (Figure S7). MDF analysis again revealed that the pathway was thermodynamically feasible when the NAD^+ concentration was between 0.1 and 5.7 mM, while acyl-ACP-hydrolase had the lowest driving force (Figure S8).

Coniferyl-aldehyde dehydrogenase involved in the phenylpropanoid biosynthesis pathway (Figure S9) in stalk was a cold stress-related bottleneck and impacted the production of ferulic acid of the stalk biomass. MDF analysis revealed that, with an NAD^+ concentration greater than 0.3 mM, the phenylpropanoid biosynthesis pathway became thermodynamically infeasible, and coniferyl-aldehyde dehydrogenase had the lowest driving force (Figure S10). Phosphohexomutase of the fructose-mannose biosynthesis pathway in the kernel was a cold stress bottleneck (Figure S11). MDF analysis showed that the fructose-mannose biosynthesis pathway was thermodynamically feasible only when the concentration of fructose 6-phosphate was between 2.5 and 5 mM. In this concentration range, phosphohexomutase was the reaction with the lowest driving force (Figure S12).

For heat stress-only metabolic bottlenecks, we focused on pyruvate-phosphate dikinase and malate dehydrogenase, both associated with the leaf photosynthetic pathway (Figure 3E), and increased the biomass growth rate by 14% each, followed by cytochrome *b*5 reductase (24%) and acyl-ACP-hydrolase (24%). MDF showed that, with an ATP concentration below 1.8 mM, the photosynthetic pathway was thermodynamically infeasible (Figure 3F). Both pyruvate-phosphate dikinase and malate dehydrogenase were combined bottlenecks when the ATP concentration was between 4.7 and 5.7 mM. A similar analysis was performed by varying the concentration of NAD^+, revealing photosynthetic pathway was thermodynamically feasible when its concentration was between of 0.1–5.7 mM. Pyruvate-phosphate dikinase and malate dehydrogenase were the combined bottleneck in this range of NAD^+ concentration. Thus, the MDF analysis connected metabolic bottlenecks with thermodynamic driving forces. Other bottleneck reactions for heat stress are listed in Table S5.

Parameter tuning of bottleneck enzymes

As the relation between bottleneck reactions and thermodynamics was consistent, we explored different parameters of corresponding enzymes to understand the nature of the bottlenecks. For that, we devised a template-based algorithm, Structure Informed enzyme turnover rate ($SI-k_{cat}$), to calculate k_{cat} (Table S6) of two common enzymes of both stress conditions (cytochrome *b*5 reductase and acyl-ACP-hydrolase), two enzymes for the heat stress (malate dehydrogenase and pyruvate-phosphate dikinase), and one enzyme for cold stress (coniferyl-aldehyde dehydrogenase). Using predicted k_{cat} values, we determined the relationship between enzyme concentration (E) and saturation (K), (Equation 18), (Figure S13). k_{cat} of an enzyme may vary depending on the compartmentalization of the enzyme (all other information such as $v_{reaction}$ and ΔG are also compartment-specific). Therefore, the accuracy of E values largely depends on the computational framework of estimating k_{cat}. $SI - k_{cat}$ is based on experimental evidence coming from maize or other closely related organisms. Thus, we expect a good accuracy of the calculated E values. For all the five enzymes, with lower enzyme saturations (0.1–0.2), higher k_{cat} reduced the required enzyme concentrations. However, once the enzyme saturation passed 0.6, the effect of different k_{cat} became lower. Thus, one strategy to improve temperature stress could be to engineer bottleneck enzymes to maintain high saturation by improving its affinity to substrates $\left(\frac{1}{k_m}\right)$.

Potential of AMF to alleviate bottlenecks: A proof of concept

Although fine-tuning between k_{cat} and K can help improve bottlenecks, it requires significant effort in designing synthetic biology tools. Instead, we can use AMFs, which are well known to alleviate different abiotic stresses in plants.[35] Among these AMFs, the effectiveness of maize inoculation with the *R. irregularis* is well studied.[11] Therefore, as a proof of concept, we generated maize root and leaf transcriptomic data from *R. irregularis* inoculated maize plants to assess the status of bottleneck reactions. In roots, 7,769 genes were differentially expressed in inoculated plants compared to control plants, among which 4,693 were upregulated (Figure 4A). Similarly, 6,639 genes were differentially expressed in leaves, among which 3,485 were upregulated (Figure 4B). In addition, 1,200 and 43 genes showed a log2 fold-change higher than 2 in roots and leaves, respectively. Gene enrichment analysis was then performed for the root genes exhibiting a log2 fold-change higher than

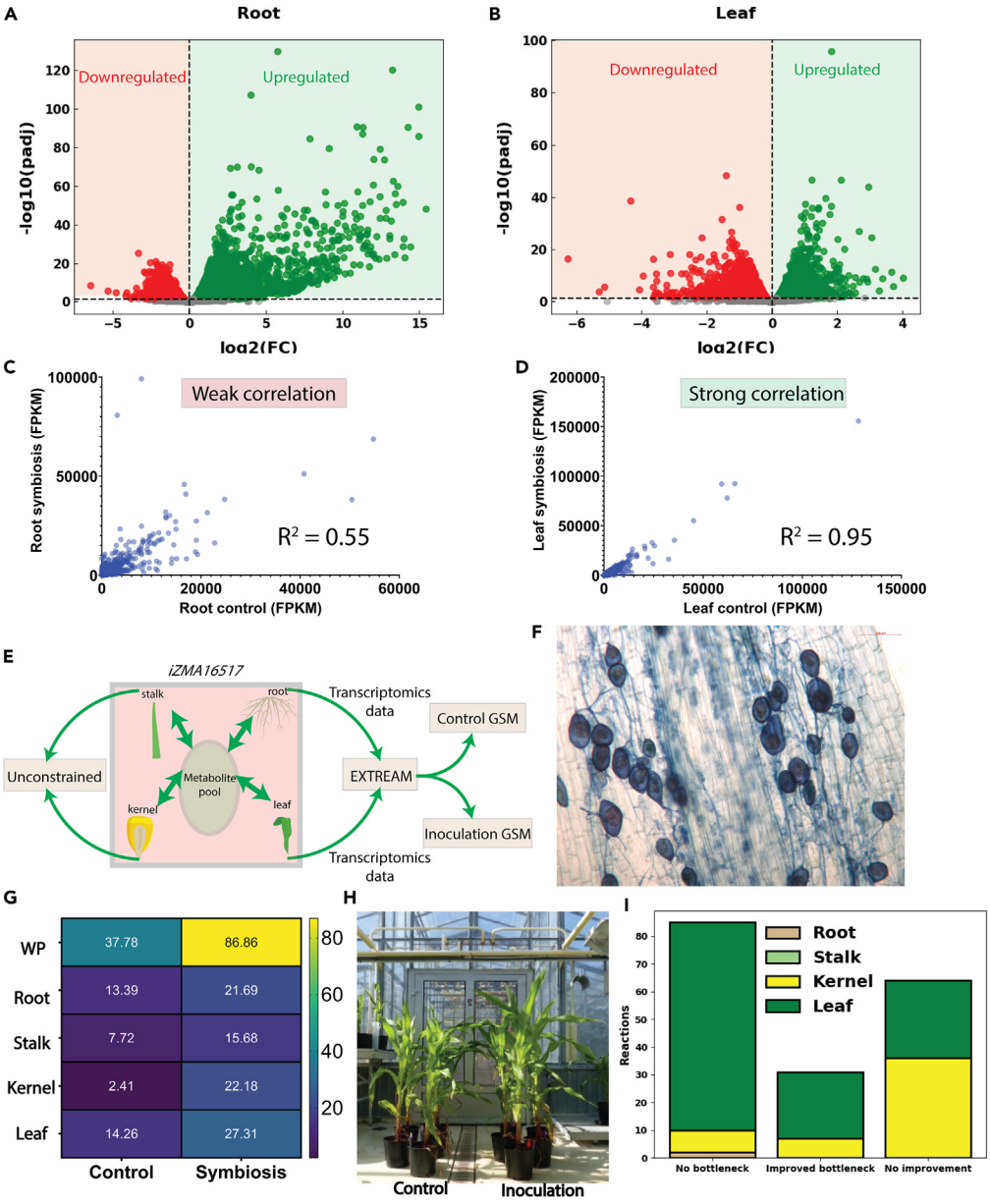

Figure 4. Maize plant responses to the AMF *R irregularis*

(A) Volcano plot of root transcriptomic data for control and inoculated plants.

(B) Volcano plot of leaf transcriptomic data for control and inoculated plants.

(C) Comparison between root transcriptomic data for control and inoculated plants.

(D) Comparison between leaf transcriptomic data for control and symbiotic conditions.

(E) Root and leaf transcriptomic data integration using the *i*ZMA6517.

(F) *R. irregularis* inoculation of maize root.

(G) Root inoculated contextualized *i*ZMA6517 predicted the pattern of biomass growth rate, matched with experimental growth pattern. WP: Whole Plant.

(H) Picture of plants used for the study displaying higher biomass under inoculation conditions compared to control.

(I) In the symbiotic interaction, 65% of bottlenecks, identified in cold stress, were alleviated.

10 (Figure S14). We found an enrichment of xylanase inhibitor protein, suggesting protection from microbial xylanase-induced hemicellulose degradation of maize roots by *R. irregularis*. A similar analysis was conducted with leaf genes exhibiting a log2 fold-change higher than 2 (Figure S15). We found a significant enrichment of pyruvate dikinase and malate dehydrogenase.[36]

We plotted root transcripts for inoculated plants and non-inoculated plants and found a relatively low correlation of 0.55, indicating a distinct transcriptional response after inoculation (Figure 4C). Alcohol dehydrogenase and pyruvate decarboxylase were significantly

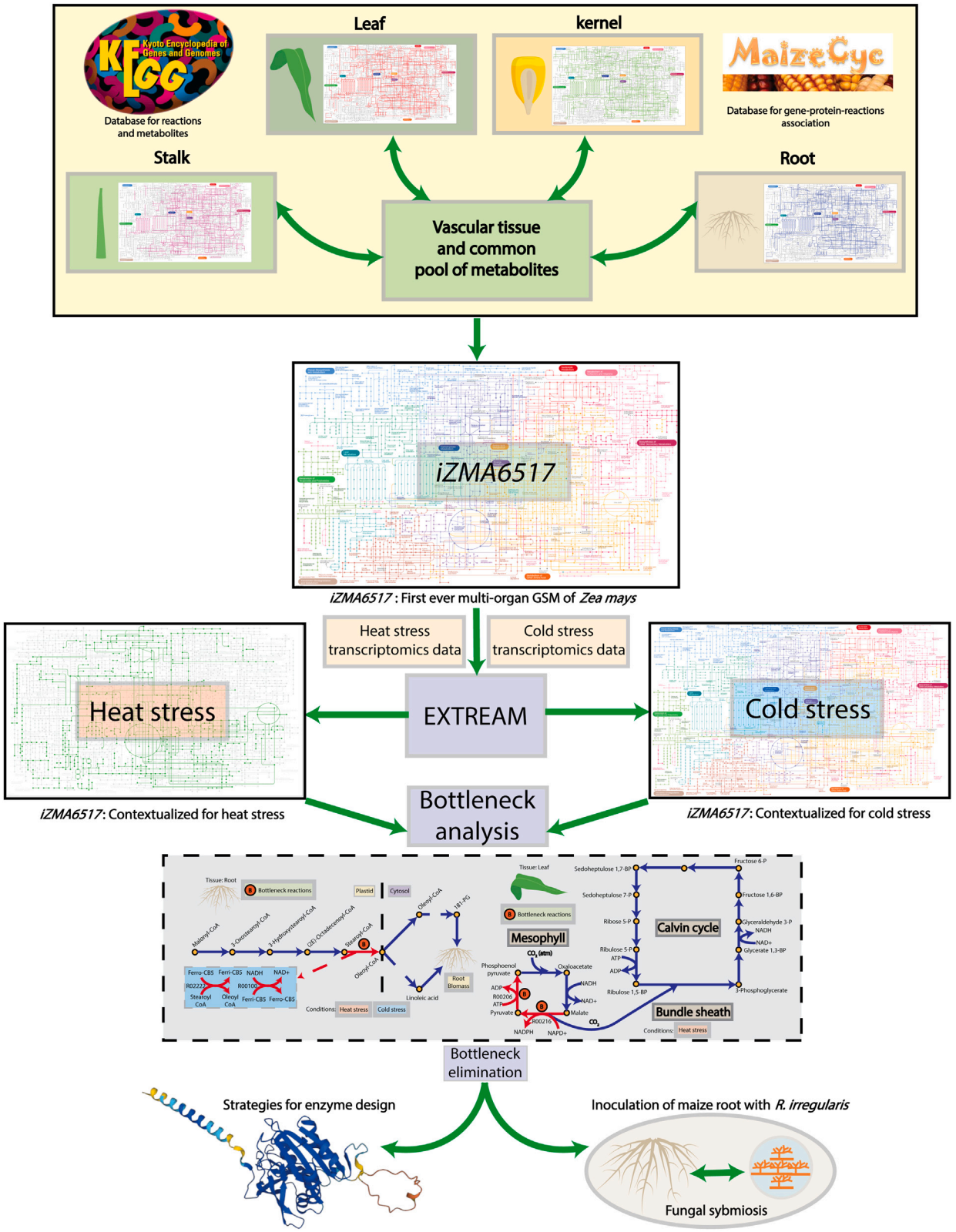
Kyoto Encyclopedia of Genes and Genomes
Database for reactions and metabolites
Leaf
kernel
MaizeCyc
Database for gene-protein-reactions association
Stalk
Root
Vascular tissue and common pool of metabolites
iZMA6517
iZMA6517 : First ever multi-organ GSM of Zea mays
Heat stress transcriptomics data
Cold stress transcriptomics data
Heat stress
EXTREAM
Cold stress
iZMA6517: Contextualized for heat stress
Bottleneck analysis
iZMA6517: Contextualized for cold stress
Tissue: Root
Bottleneck reactions
Plastid
Cytosol
Malonyl-CoA
3-Oxostearoyl-CoA
3-Hydroxystearoyl-CoA
2(E)-Octadecenoyl-CoA
Stearoyl-CoA
Oleoyl-CoA
18:1-PG
Linoleic acid
Root Biomass
Ferro-CBS
Ferri-CBS
NADH
NAD+
R02227
R00100
Stearoyl CoA
Oleoyl CoA
Conditions: Heat stress Cold stress
Tissue: Leaf
Mesophyll
Phosphoenol pyruvate
Oxaloacetate
ADP
ATP
R00206
Pyruvate
Malate
R00216
NADPH
NAPD+
Sedoheptulose 1,7-BP
Sedoheptulose 7-P
Ribose 5-P
Ribulose 5-P
Ribulose 1,5-BP
Calvin cycle
Fructose 6-P
Fructose 1,6-BP
Glyceraldehyde 3-P
Glycerate 1,3-BP
3-Phosphoglycerate
Bundle sheath
Conditions: Heat stress
Bottleneck elimination
Strategies for enzyme design
Inoculation of maize root with R. irregularis
Fungal sybmiosis

Figure 5. Overall workflow of this project

We reconstructed the first ever multi-organ GSM of maize, *i*ZMA6517. We integrated heat and cold stress transcriptomics data with *i*ZMA6517 with the EXTREAM. Later, we devised MBA to find metabolic bottlenecks of heat and cold stress conditions. We showed that, metabolic bottlenecks on both conditions are guided by thermodynamic principles. We then proposed protein engineering strategies to improve metabolic bottlenecks. Finally, we showed that *R. irregularis* symbiosis with maize root can also alleviate major metabolic bottlenecks.

upregulated in the symbiosis. For leaves, we found a strong correlation of 0.95, indicating a similar transcriptomic response in the plants inoculated with *R. irregularis* compared to the control (Figure 4D).

As leaf and root tissues were most affected by the temperature stress, we used these transcriptomics data to reconstruct contextualized *i*ZMA6517s for control and inoculated plants using EXTREAM (Figure 4E). As these models were not constrained for kernel and stalk, it enabled us to find all theoretical temperature stress alleviation strategies for these two organs. Next, from contextualized models, we found, both whole plant biomass and organ-specific biomass growth rates were higher in the inoculated plants (Figures 4F–4H). Subsequently, implementing MBA to the symbiosis model showed that all the cold stress bottleneck reactions were alleviated. For heat stress, 85 out of 180 (47%) bottleneck reactions were no longer bottlenecks following inoculation (Figure 4I). Moreover, 31 bottleneck reactions (18%) showed improvement in inoculated plants. Finally, 64 bottleneck reactions (35%) did not show improvement upon inoculation. However, out of those 64 reactions, 62 had a minimal (1–3%) impact on biomass growth rate, except for pyruvate kinase in two different pyruvate 2-*O*-phosphotransferase of the leaf (8% and 7%), (Table S7). Thus, inoculation with *R. irregularis* has the potential to alleviate temperature stress.

DISCUSSION

Climate change, causing temperature stress, is a leading cause of reduced maize production.[37] Here, we introduced *i*ZMA6517, a multi-organ maize GSM, to better understand the maize metabolism under temperature stress. Figure 5 shows the overall workflow of this study.

In first-generation plant GSMs, all organ-specific reactions were combined into a single multi-compartment model. Example of such GSMs are AraGEM,[38] C4GEM,[39] and *i*RS1563.[40] However, these models were unable to simulate inter-organ interactions. The first multi-organ GSM was reconstructed for barley,[12] and subsequently for other plants (see introduction). However, apart from a core arabidopsis GSM,[15] none of the multi-organ GSMs included root, stalk, kernel, and leaf (Table S8). *i*ZMA6517 is the only model thus far combining these four organ-specific GSMs with finer resolution (Figure S16), making it the most comprehensive multi-organ plant GSM.

The E-flux algorithm predicted accurate root phenotype under nitrogen starvation.[19] However, it could not predict the carbohydrate profile in the leaf (Figure 1F). We hypothesized that the solution space of the E-flux algorithm was overly permissive, resulting in an inaccurate carbohydrate profile. Thus, we further restricted the feasible solution space by equally distributing the transcript of each gene based on the number of reactions the gene participated in. The objective function was to minimize the sum of reaction fluxes compared to a reference condition, calculated from the transcriptomic data. A similar objective function was used in MOMA.[41] However, MOMA used wild-type flux distribution as the reference to estimate flux distribution after gene knockouts. In our case, the purpose of the reference condition was to maximize agreement between transcriptomic data and reaction flux. After these modifications, the new algorithm, EXTREAM, predicted the correct carbohydrate profile across leaf cross-sections. We also wanted to check which aspect of EXTREAM contributed more toward the correct prediction of starch distribution. To address that, we formulated two different optimization problems. In one optimization problem (OPT-01), we used the distributed transcriptomics data with biomass maximization, and in the other optimization problem (OPT-02), we used non-distributed transcriptomics data with the modified objective function. OPT-01 predicted the right starch distribution, whereas OPT-02 predicted inaccurate starch distribution. Thereby transcript distribution played a crucial role in the correct prediction of starch profile. The optimization problems can be accessed through the GitHub directory (data and code availability section).

After contextualizing *i*ZMA6517 with EXTREAM, we devised MBA to find plant-wide metabolic bottlenecks. MBA identifies bottleneck reactions in a given metabolic network by expanding the flux space of each reaction to a maximum possible value individually and assess its impact on the biomass growth rate. Compared to the shadow price analysis, which is a metabolite-centric approach, MBA is a reaction-centric approach and better suited for metabolic engineering/bottleneck identification purpose. Under heat stress, 180 reactions were identified as metabolic bottlenecks, whereas only 5 metabolic bottlenecks were identified under cold stress, revealing a fundamental difference between both stresses. This finding can explain the weak transcriptomic correlation between heat and cold stresses (Figure 1C). MBA indicated that leaf tissue hosted most bottleneck reactions under heat stress (Figure 3A), consistent with previous works.[42] For cold stress, root tissue hosted most bottleneck reactions (Figure 3A), also confirmed by an earlier study.[43] To further understand both stresses, we analyzed heat stress bottleneck reactions and 17% of those (Table S9) were associated with NAD+/NADH pair, suggesting a relationship between reducing power and heat stress. Additionally, 25% of the bottleneck reactions (Table S10) were associated with ADP/ATP pairs. Thus, heat stress is driven by two major components, reducing power and energy generation. Previous studies independently confirmed the effect of reducing power[44] and energy generation[45] on heat stress. However, this work showed the synergistic impact of both metabolic components on heat stress. A similar analysis on cold stress bottleneck reactions revealed 60% of those were associated with NAD+/NADH (Table S11). Surprisingly, none of the reactions were related to the ADP/ATP pair. Previous studies also confirmed the effect of reducing power on cold stress.[46] We performed the MDF analysis to find common features behind the interplay of reducing power and energy generation. The analysis found all the tested reactions can be the thermodynamic bottlenecks in their respective pathways, revealing a multi-faceted characteristic of temperature stress, geared by the thermodynamics-reducing power-energy generation axis. Literature evidence suggested that cytochrome *b*5 reductase (one of the two bottleneck enzymes on both stresses) of arabidopsis mutant had lower growth than the wild type.[47] A similar

observation was made for acyl-ACP-hydrolase (another common bottleneck enzyme under both heat and cold stress) for arabidopsis.[48] These evidences further validate the proposed thermodynamics-reducing power-energy generation axis.

Enzymes are increasingly repurposed by rational design for directed evolution. Enzyme turnover rate (k_{cat}) and saturation (K) are common parameters for such rational design.[49] A previous work[50] established a relation among enzyme concentration (E), k_{cat}, and K. To explore the relationship for bottleneck enzymes mentioned in the result section, reliable values of k_{cat} are needed, based on which, E can be calculated. There is a deep learning-based algorithm[51] that can predict k_{cat}; however, for maize, the algorithm returned k_{cat} values, not in good agreement with the literature (Figures S17–S21). Thus, we proposed a structural similarity weightage-based algorithm ($SI - k_{cat}$), which predicted k_{cat} values of enzymes, close to experimental observations. With the new k_{cat} values, we sampled the different enzyme saturation to calculate E. For all the tested enzymes, the effect of k_{cat} was prevalent in the lower K (Figure S16). However, with the increasing K, the effect of k_{cat} became less. Hence, a strategy for rational enzyme design for alleviating temperature stress can be to implement directed evolution for heat/cold stress to fine-tune the relationship between $k_{cat} - K$.

A practical approach to alleviating abiotic stress can be to inoculate maize root with an AMF such as *R. irregularis*.[35,52–54] Previous work indicated that AMF inoculated C_4 plant species exhibited better abiotic stress tolerance through improved quantum yield of PSII, thus providing additional electron sinks.[55] Moreover, AMF improves plant nutrition by increasing availability and translocation of numerous nutrients.[56] AMF also improves soil quality by changing its properties, which contributes in improving plant health.[57] Hyphae of AMF can hasten the breakdown of organic materials in soil and can make more nutrients available to roots.[58] Furthermore, mycorrhizal fungi may influence ambient CO_2 fixation of host plants by boosting "sink effect" and photo assimilate transport from aerial portions to roots. Thus, as a proof of concept, we generated transcriptomic data for control and AMF inoculated maize and reconstructed GSMs for both conditions to assess the status of bottleneck reactions. Inoculation GSM predicted a higher biomass growth rate for all tissues (Figure 4F). Moreover, we predicted that the inoculation alleviated all cold stress and 65% heat stress reactions. We also calculated flux sum, a proxy for metabolite concentration, for NAD+ and found 49% (Figure S22) increase in the inoculation condition, indicating an additional availability of electron sink provided by the inoculation with *R. irregularis*, which can potentially help maize overcoming the temperature stress. However, *R. irregularis* symbiosis still had bottlenecks from purine, pyruvate, pyrimidine, folate, and fatty acid metabolism (Table S12; Figure S23). Additional improvements of the plant biomass production can be achieved by debottlenecking these reactions.

Overall, the first muti-organ maize GSM, *i*ZMA6517, with the aid of EXTREAM and MBA, dissected the impact of temperature stress on maize. Our analysis revealed three major conclusions: (1) heat and cold stresses are fundamentally different; (2) both stresses are associated with reducing power, while heat stress has additional bottlenecks in energy generation; and (3) inoculation with *R. irregularis* can be an effective way to alleviate temperature stress. Using these inferences, a better temperature stress-tolerant maize ideotype with an improved grain yield can be designed. Future work can be extended to elucidate the plant-wide impact of different other abiotic stresses and how abiotic stresses can be ameliorated with the inoculation of AMF. One such case can be to assess the plant-wide impact of *R. irregularis* under high and low nitrogen conditions. This work is currently underway with promising predictions from *i*ZMA6517.

Limitations of the study

There are a few limitations of this study. Starting from the model reconstruction process, the biomass composition used for individual organs were collected from different literature, mostly from the unstressed conditions. However, in an ideal scenario, for each organ, there should have been three different biomass equation—one for control condition, one for heat stress condition, and another one for cold stress condition. This indicates, still many aspects of temperature stress is unexplored for maize. For MBA, although we pinpointed plant-wide metabolic bottleneck in both heat and cold stresses, we could not perform *in vivo* experimentation to verify those. Future efforts will be dedicated toward verifying those bottlenecks. Finally, although as a proof-of-concept, we showed *R. irregularis* could alleviate temperature stress, we could not induce temperature stress with symbiosis study. Future experimentations will be geared toward that.

STAR★METHODS

Detailed methods are provided in the online version of this paper and include the following:

- KEY RESOURCES TABLE
- RESOURCE AVAILABILITY
  - Lead contact
  - Materials availability
  - Data and code availability
- EXPERIMENTAL MODEL AND SUBJECT DETAILS
  - Plant experiments
- METHOD DETAILS
  - K-means clustering analysis
  - Genome-scale metabolic model reconstruction
  - EXpression disTributed REAction flux Measurement algorithm
  - MBA
  - Min/Max Driving Force analysis

SUPPLEMENTAL INFORMATION

Supplemental information can be found online at https://doi.org/10.1016/j.isci.2023.108400.

ACKNOWLEDGMENTS

R.S. gratefully acknowledges funding support from National Science Foundation (NSF) CAREER grant (1943310) and Nebraska Collaboration Initiative Grant (21-1106-6011). C.D.M. acknowledges partial support by the Center for Bioenergy Innovation, a U.S. Department of Energy Bioenergy Research Center supported by the Office of Biological and Environmental Research in the DOE Office of Science. R.C. thanks Iowa State University startup, Translation AI Center Seed Grant, and National Science Foundation under Grant No. (2242763) EPSCoR RII Track-1. A.D. acknowledges the support from Plant2Pro by the French National Agency for Research - ANR (agreement #18-CARN-024-01 – 2018). A.D. also acknowledges the benefits received from France 2030 program (Saclay Plant Sciences, reference n° ANR-17-EUR-0007, EUR SPS-GSR integrated into France 2030 (reference n° ANR-11-IDEX-0003-02), INRAE Grant IB BAP 2021 MYCORN, and IJPB's Plant Observatory technological platforms. We thank Michel Lebrusque, Lilan Diahuron, Patrick Grillot, and Christian Jeudy for taking care of the plants in the greenhouse. We thank the POPS platform for the RNAseq experiment and data. We also thank Etienne Delannoy, Christine Paysant le Roux, and Alexandra Launay-Avon from POPS platform for fruitful discussions. We are grateful to Cyril Bauland and Carine Palaffre from the INRAE for providing B73 seeds from the Centre de Ressources Biologiques of Saint Martin de Hinx (France). The original B73 seeds were provided by the North Central Regional Plant Introduction Station (IA, USA) for whom we are grateful.

AUTHOR CONTRIBUTIONS

R.S., C.D.M., A.D., R.C., and B.H. conceived the study and edited the manuscript. N.B.C. wrote the original manuscript. N.B.C. reconstructed and curated the model. K.A.S. and B.A. generated the k_{cat} values. N.B.C. and M.S. performed computational analyses. B.D. performed the experiments on the inoculation study. I.Q. was involved in experimental design and plant care. M.R. was involved in plant growth and care, and monitoring RNA extractions.

DECLARATION OF INTERESTS

The authors declare no competing interests.

Received: August 7, 2023
Revised: October 30, 2023
Accepted: November 3, 2023
Published: November 7, 2023

REFERENCES

1. Zhang, Y., and Zhao, Y. (2017). Ensemble yield simulations: Using heat-tolerant and later-maturing varieties to adapt to climate warming. PLoS One *12*, e0176766.
2. Yu, T., Zhang, J., Cao, J., Cai, Q., Li, X., Sun, Y., Li, S., Li, Y., Hu, G., Cao, S., et al. (2021). Leaf transcriptomic response mediated by cold stress in two maize inbred lines with contrasting tolerance levels. Genomics *113*, 782–794. https://doi.org/10.1016/j.ygeno.2021.01.018.
3. Guo, J., Gu, X., Lu, W., and Lu, D. (2021). Multiomics analysis of kernel development in response to short-term heat stress at the grain formation stage in waxy maize. J. Exp. Bot. *72*, 6291–6304. https://doi.org/10.1093/jxb/erab286.
4. Xuhui, L., Weiwei, C., Siqi, L., Junteng, F., Hang, Z., Xiangbo, Z., and Yongwen, Q. (2022). Full-length transcriptome analysis of maize root tips reveals the molecular mechanism of cold stress during the seedling stage. BMC Plant Biol. *22*, 398. https://doi.org/10.1186/s12870-022-03787-3.
5. Shao, J., Liu, P., Zhao, B., Zhang, J., Zhao, X., and Ren, B. (2023). Combined effects of high temperature and waterlogging on yield and stem development of summer maize. Crop J. *11*, 651–660. https://doi.org/10.1016/j.cj.2022.08.005.
6. Moore, C.E., Meacham-Hensold, K., Lemonnier, P., Slattery, R.A., Benjamin, C., Bernacchi, C.J., Lawson, T., and Cavanagh, A.P. (2021). The effect of increasing temperature on crop photosynthesis: from enzymes to ecosystems. J. Exp. Bot. *72*, 2822–2844. https://doi.org/10.1093/jxb/erab090.
7. Tian, Y., Chen, J., Chen, C., Deng, A., Song, Z., Zheng, C., Hoogmoed, W., and Zhang, W. (2012). Warming impacts on winter wheat phenophase and grain yield under field conditions in Yangtze Delta Plain, China. F. Crop. Res. *134*, 193–199. https://doi.org/10.1016/j.fcr.2012.05.013.
8. Khan, A.H., Ma, Y., Wu, Y., Akbar, A., Shaban, M., Ullah, A., Deng, J., Khan, A.S., Chi, H., Zhu, L., et al. (2023). High-temperature stress suppresses allene oxide cyclase 2 and causes male sterility in cotton by disrupting jasmonic acid signaling. Crop J. *11*, 33–45. https://doi.org/10.1016/j.cj.2022.05.009.
9. Wu, Y., Li, X., Li, Y., Ma, H., Chi, H., Ma, Y., Yang, J., Xie, S., Zhang, R., Liu, L., et al. (2022). Degradation of de-esterified pctin/homogalacturonan by the polygalacturonase GhNSP is necessary for pollen exine formation and male fertility in cotton. Plant Biotechnol. J. *20*, 1054–1068. https://doi.org/10.1111/pbi.13785.
10. Zhang, R., Zhou, L., Li, Y., Ma, H., Li, Y., Ma, Y., Lv, R., Yang, J., Wang, W., Alifu, A., et al. (2022). Rapid Identification of Pollen- and Anther-Specific Genes in Response to High-Temperature Stress Based on Transcriptome Profiling Analysis in Cotton. Int. J. Mol. Sci. *23*, 3378. https://doi.org/10.3390/ijms23063378.

11. Zhu, X.-C., Song, F.-B., Liu, S.-Q., and Liu, T.-D. (2011). Effects of arbuscular mycorrhizal fungus on photosynthesis and water status of maize under high temperature stress. Plant Soil *346*, 189–199. https://doi.org/10.1007/s11104-011-0809-8.
12. Grafahrend-Belau, E., Junker, A., Eschenröder, A., Müller, J., Schreiber, F., and Junker, B.H. (2013). Multiscale Metabolic Modeling: Dynamic Flux Balance Analysis on a Whole-Plant Scale. Plant Physiol. *163*, 637–647. https://doi.org/10.1104/pp.113.224006.
13. Pfau, T., Christian, N., Masakapalli, S.K., Sweetlove, L.J., Poolman, M.G., and Ebenhöh, O. (2018). The intertwined metabolism during symbiotic nitrogen fixation elucidated by metabolic modelling. Sci. Rep. *8*, 12504. https://doi.org/10.1038/s41598-018-30884-x.
14. Shaw, R., and Cheung, C.Y.M. (2018). A Dynamic Multi-Tissue Flux Balance Model Captures Carbon and Nitrogen Metabolism and Optimal Resource Partitioning During Arabidopsis Growth. Front. Plant Sci. *9*, 884.
15. Schroeder, W.L., and Saha, R. (2020). Introducing an Optimization- and explicit Runge-Kutta- based Approach to Perform Dynamic Flux Balance Analysis. Sci. Rep. *10*, 9241. https://doi.org/10.1038/s41598-020-65457-4.
16. Moreira, T.B., Shaw, R., Luo, X., Ganguly, O., Kim, H.-S., Coelho, L.G.F., Cheung, C.Y.M., and Rhys Williams, T.C. (2019). A Genome-Scale Metabolic Model of Soybean (Glycine max) Highlights Metabolic Fluxes in Seedlings. Plant Physiol. *180*, 1912–1929. https://doi.org/10.1104/pp.19.00122.
17. Shaw, R., and Cheung, C.Y.M. (2019). A mass and charge balanced metabolic model of Setaria viridis revealed mechanisms of proton balancing in C4 plants. BMC Bioinf. *20*, 357–411. https://doi.org/10.1186/s12859-019-2941-z.
18. Shaw, R., and Cheung, C.Y.M. (2021). Integration of crop growth model and constraint-based metabolic model predicts metabolic changes over rice plant development under water-limited stress. In Silico Plants *3*, diab020. https://doi.org/10.1093/insilicoplants/diab020.
19. Chowdhury, N.B., Schroeder, W.L., Sarkar, D., Amiour, N., Quilleré, I., Hirel, B., Maranas, C.D., and Saha, R. (2022). Dissecting the metabolic reprogramming of maize root under nitrogen-deficient stress conditions. J. Exp. Bot. *73*, 275–291. https://doi.org/10.1093/jxb/erab435.
20. Song, H.-S., Reifman, J., and Wallqvist, A. (2014). Prediction of Metabolic Flux Distribution from Gene Expression Data Based on the Flux Minimization Principle. PLoS One *9*, e112524.
21. Kim, M.K., and Lun, D.S. (2014). Methods for integration of transcriptomic data in genome-scale metabolic models. Comput. Struct. Biotechnol. J. *11*, 59–65. https://doi.org/10.1016/j.csbj.2014.08.009.
22. Makarevitch, I., Waters, A.J., West, P.T., Stitzer, M., Hirsch, C.N., Ross-Ibarra, J., and Springer, N.M. (2015). Transposable Elements Contribute to Activation of Maize Genes in Response to Abiotic Stress. PLoS Genet. *11*, e1004915.
23. Nguyen, H.T., Leipner, J., Stamp, P., and Guerra-Peraza, O. (2009). Low temperature stress in maize (Zea mays L.) induces genes involved in photosynthesis and signal transduction as studied by suppression subtractive hybridization. Plant Physiol. Biochem. *47*, 116–122. https://doi.org/10.1016/j.plaphy.2008.10.010.
24. Perdomo, J.A., Capó-Bauçà, S., Carmo-Silva, E., and Galmés, J. (2017). Rubisco and Rubisco Activase Play an Important Role in the Biochemical Limitations of Photosynthesis in Rice, Wheat, and Maize under High Temperature and Water Deficit. Front. Plant Sci. *8*, 490.
25. Colijn, C., Brandes, A., Zucker, J., Lun, D.S., Weiner, B., Farhat, M.R., Cheng, T.Y., Moody, D.B., Murray, M., and Galagan, J.E. (2009). Interpreting expression data with metabolic flux models: Predicting Mycobacterium tuberculosis mycolic acid production. PLoS Comput. Biol. *5*, e1000489. https://doi.org/10.1371/journal.pcbi.1000489.
26. Wang, L., Czedik-Eysenberg, A., Mertz, R.A., Si, Y., Tohge, T., Nunes-Nesi, A., Arrivault, S., Dedow, L.K., Bryant, D.W., Zhou, W., et al. (2014). Comparative analyses of C4 and C3 photosynthesis in developing leaves of maize and rice. Nat. Biotechnol. *32*, 1158–1165. https://doi.org/10.1038/nbt.3019.
27. Simons, M., Saha, R., Amiour, N., Kumar, A., Guillard, L., Clément, G., Miquel, M., Li, Z., Mouille, G., Lea, P.J., et al. (2014). Assessing the metabolic impact of nitrogen availability using a compartmentalized maize leaf genome-scale model. Plant Physiol. *166*, 1659–1674. https://doi.org/10.1104/pp.114.245787.
28. Schroeder, W.L., and Saha, R. (2020). OptFill: A Tool for Infeasible Cycle-Free Gapfilling of Stoichiometric Metabolic Models. iScience *23*, 100783. https://doi.org/10.1016/j.isci.2019.100783.
29. Monaco, M.K., Sen, T.Z., Dharmawardhana, P.D., Ren, L., Schaeffer, M., Naithani, S., Amarasinghe, V., Thomason, J., Harper, L., Gardiner, J., et al. (2013). Maize Metabolic Network Construction and Transcriptome Analysis. Plant Genome *6*, 1–12. https://doi.org/10.3835/plantgenome2012.09.0025.
30. Cañas, R.A., Quilleré, I., Christ, A., and Hirel, B. (2009). Nitrogen metabolism in the developing ear of maize (Zea mays): analysis of two lines contrasting in their mode of nitrogen management. New Phytol. *184*, 340–352. https://doi.org/10.1111/j.1469-8137.2009.02966.x.
31. Mishra, P.K., Bisht, S.C., Ruwari, P., Selvakumar, G., Joshi, G.K., Bisht, J.K., Bhatt, J.C., and Gupta, H.S. (2011). Alleviation of cold stress in inoculated wheat (Triticum aestivum L.) seedlings with psychrotolerant Pseudomonads from NW Himalayas. Arch. Microbiol. *193*, 497–513. https://doi.org/10.1007/s00203-011-0693-x.
32. Waqas, M.A., Wang, X., Zafar, S.A., Noor, M.A., Hussain, H.A., Azher Nawaz, M., and Farooq, M. (2021). Thermal Stresses in Maize: Effects and Management Strategies. Plants *10*, 293. https://doi.org/10.3390/plants10020293.
33. Noor, E., Bar-Even, A., Flamholz, A., Reznik, E., Liebermeister, W., and Milo, R. (2014). Pathway Thermodynamics Highlights Kinetic Obstacles in Central Metabolism. PLoS Comput. Biol. *10*, e1003483.
34. Beber, M.E., Gollub, M.G., Mozaffari, D., Shebek, K.M., Flamholz, A.I., Milo, R., and Noor, E. (2022). eQuilibrator 3.0: a database solution for thermodynamic constant estimation. Nucleic Acids Res. *50*, D603–D609. https://doi.org/10.1093/nar/gkab1106.
35. Lenoir, I., Fontaine, J., and Lounès-Hadj Sahraoui, A. (2016). Arbuscular mycorrhizal fungal responses to abiotic stresses: A review. Phytochemistry *123*, 4–15. https://doi.org/10.1016/j.phytochem.2016.01.002.
36. Balestrini, R., Brunetti, C., Chitarra, W., and Nerva, L. (2020). Photosynthetic Traits and Nitrogen Uptake in Crops: Which Is the Role of Arbuscular Mycorrhizal Fungi? Plants *9*, 1105. https://doi.org/10.3390/plants9091105.
37. Cairns, J.E., Sonder, K., Zaidi, P.H., Verhulst, N., Mahuku, G., Babu, R., Nair, S.K., Das, B., Govaerts, B., Vinayan, M.T., et al. (2012). Chapter one - Maize Production in a Changing Climate: Impacts, Adaptation, and Mitigation Strategies. In Advances in Agronomy, D.L. Sparks, ed. (Academic Press), pp. 1–58.
38. Dal'Molin, C.G. de O., Quek, L.E., Palfreyman, R.W., Brumbley, S.M., and Nielsen, L.K. (2010). AraGEM, a genome-scale reconstruction of the primary metabolic network in Arabidopsis. Plant Physiol. *152*, 579–589. https://doi.org/10.1104/pp.109.148817.
39. de Oliveira Dal'Molin, C.G., Quek, L.-E., Palfreyman, R.W., Brumbley, S.M., and Nielsen, L.K. (2010). C4GEM, a Genome-Scale Metabolic Model to Study C4 Plant Metabolism. Plant Physiol. *154*, 1871–1885. https://doi.org/10.1104/pp.110.166488.
40. Saha, R., Suthers, P.F., and Maranas, C.D. (2011). Zea mays irs1563: A comprehensive genome-scale metabolic reconstruction of maize metabolism. PLoS One *6*, e21784. https://doi.org/10.1371/journal.pone.0021784.
41. Segrè, D., Vitkup, D., and Church, G.M. (2002). Analysis of optimality in natural and perturbed metabolic networks. Proc. Natl. Acad. Sci. USA *99*, 15112–15117. https://doi.org/10.1073/pnas.232349399.
42. El-Sappah, A.H., Rather, S.A., Wani, S.H., Elrys, A.S., Bilal, M., Huang, Q., Dar, Z.A., Elashtokhy, M.M.A., Soaud, N., Koul, M., et al. (2022). Heat Stress-Mediated Constraints in Maize (Zea mays) Production: Challenges and Solutions. Front. Plant Sci. *13*, 879366.
43. Hund, A., Richner, W., Soldati, A., Fracheboud, Y., and Stamp, P. (2007). Root morphology and photosynthetic performance of maize inbred lines at low temperature. Eur. J. Agron. *27*, 52–61. https://doi.org/10.1016/j.eja.2007.01.003.
44. Kumar, S., Gupta, D., and Nayyar, H. (2012). Comparative response of maize and rice genotypes to heat stress: status of oxidative stress and antioxidants. Acta Physiol. Plant. *34*, 75–86. https://doi.org/10.1007/s11738-011-0806-9.
45. Begcy, K., Nosenko, T., Zhou, L.-Z., Fragner, L., Weckwerth, W., and Dresselhaus, T. (2019). Male Sterility in Maize after Transient Heat Stress during the Tetrad Stage of Pollen Development1 [OPEN]. Plant Physiol. *181*, 683–700. https://doi.org/10.1104/pp.19.00707.
46. Prasad, T.K., Anderson, M.D., Martin, B.A., and Stewart, C.R. (1994). Evidence for Chilling-Induced Oxidative Stress in Maize Seedlings and a Regulatory Role for Hydrogen Peroxide. Plant Cell *6*, 65–74. https://doi.org/10.1105/tpc.6.1.65.
47. Wayne, L.L., Wallis, J.G., Kumar, R., Markham, J.E., and Browse, J. (2013). Cytochrome b5 Reductase Encoded by CBR1 Is Essential for a Functional Male Gametophyte in Arabidopsis. Plant Cell *25*, 3052–3066. https://doi.org/10.1105/tpc.113.113324.
48. Bonaventure, G., Salas, J.J., Pollard, M.R., and Ohlrogge, J.B. (2003). Disruption of the

FATB Gene in Arabidopsis Demonstrates an Essential Role of Saturated Fatty Acids in Plant Growth. Plant Cell *15*, 1020–1033. https://doi.org/10.1105/tpc.008946.

49. Hanson, A.D., McCarty, D.R., Henry, C.S., Xian, X., Joshi, J., Patterson, J.A., García-García, J.D., Fleischmann, S.D., Tivendale, N.D., and Millar, A.H. (2021). The number of catalytic cycles in an enzyme's lifetime and why it matters to metabolic engineering. Proc. Natl. Acad. Sci. USA *118*, e2023348118. https://doi.org/10.1073/pnas.2023348118.
50. Noor, E., Flamholz, A., Liebermeister, W., Bar-Even, A., and Milo, R. (2013). A note on the kinetics of enzyme action: A decomposition that highlights thermodynamic effects. FEBS Lett. *587*, 2772–2777. https://doi.org/10.1016/j.febslet.2013.07.028.
51. Li, F., Yuan, L., Lu, H., Li, G., Chen, Y., Engqvist, M.K.M., Kerkhoven, E.J., and Nielsen, J. (2022). Deep learning-based kcat prediction enables improved enzyme-constrained model reconstruction. Nat. Catal. *5*, 662–672. https://doi.org/10.1038/s41929-022-00798-z.
52. Chu, Q., Wang, X., Yang, Y., Chen, F., Zhang, F., and Feng, G. (2013). Mycorrhizal responsiveness of maize (Zea mays L.) genotypes as related to releasing date and available P content in soil. Mycorrhiza *23*, 497–505. https://doi.org/10.1007/s00572-013-0492-0.
53. Li, S., Yang, W., Guo, J., Li, X., Lin, J., and Zhu, X. (2020). Changes in photosynthesis and respiratory metabolism of maize seedlings growing under low temperature stress may be regulated by arbuscular mycorrhizal fungi. Plant Physiol. Biochem. *154*, 1–10. https://doi.org/10.1016/j.plaphy.2020.05.025.
54. Hajiboland, R., Joudmand, A., Aliasgharzad, N., Tolrá, R., Poschenrieder, C., Hajiboland, R., Joudmand, A., Aliasgharzad, N., Tolrá, R., and Poschenrieder, C. (2019). Arbuscular mycorrhizal fungi alleviate low-temperature stress and increase freezing resistance as a substitute for acclimation treatment in barley. Crop Pasture Sci. *70*, 218–233. https://doi.org/10.1071/CP18385.
55. Jajoo, A., and Mathur, S. (2021). Role of arbuscular mycorrhizal fungi as an underground saviuor for protecting plants from abiotic stresses. Physiol. Mol. Biol. Plants *27*, 2589–2603. https://doi.org/10.1007/s12298-021-01091-2.
56. Rouphael, Y., Franken, P., Schneider, C., Schwarz, D., Giovannetti, M., Agnolucci, M., Pascale, S.D., Bonini, P., and Colla, G. (2015). Arbuscular mycorrhizal fungi act as biostimulants in horticultural crops. Sci. Hortic. (Amsterdam) *196*, 91–108. https://doi.org/10.1016/j.scienta.2015.09.002.
57. Thirkell, T.J., Charters, M.D., Elliott, A.J., Sait, S.M., and Field, K.J. (2017). Are mycorrhizal fungi our sustainable saviours? Considerations for achieving food security. J. Ecol. *105*, 921–929. https://doi.org/10.1111/1365-2745.12788.
58. Paterson, E., Sim, A., Davidson, J., and Daniell, T.J. (2016). Arbuscular mycorrhizal hyphae promote priming of native soil organic matter mineralisation. Plant Soil *408*, 243–254. https://doi.org/10.1007/s11104-016-2928-8.
59. Ahmad, A., and Dey, L. (2007). A k-mean clustering algorithm for mixed numeric and categorical data. Data Knowl. Eng. *63*, 503–527. https://doi.org/10.1016/j.datak.2007.03.016.
60. Downs, G.S., Bi, Y.M., Colasanti, J., Wu, W., Chen, X., Zhu, T., Rothstein, S.J., and Lukens, L.N. (2013). A developmental transcriptional network for maize defines coexpression modules. Plant Physiol. *161*, 1830–1843. https://doi.org/10.1104/pp.112.213231.
61. Chan, S.H.J., Cai, J., Wang, L., Simons-Senftle, M.N., and Maranas, C.D. (2017). Standardizing biomass reactions and ensuring complete mass balance in genome-scale metabolic models. Bioinformatics *33*, 3603–3609. https://doi.org/10.1093/bioinformatics/btx453.
62. McCree, K.J., and Troughton, J.H. (1966). Prediction of Growth Rate at Different Light Levels from Measured Photosynthesis and Respiration Rates. Plant Physiol. *41*, 559–566. https://doi.org/10.1104/pp.41.4.559.
63. Oaks, A. (1967). Synthesis of macromolecules in maize root tips. Can. J. Bot. *45*, 385–394. https://doi.org/10.1139/b67-038.
64. Roberts, J.K., Lane, A.N., Clark, R.A., and Nieman, R.H. (1985). Relationships between the rate of synthesis of ATP and the concentrations of reactants and products of ATP hydrolysis in maize root tips, determined by 31P nuclear magnetic resonance. Arch. Biochem. Biophys. *240*, 712–722. https://doi.org/10.1016/0003-9861(85)90080-3.
65. Vuletić, M., Hadži-Tašković Šukalović, V., Marković, K., Kravić, N., Vučinić, Ž., and Maksimović, V. (2014). Differential response of antioxidative systems of maize (Zea mays L.) roots cell walls to osmotic and heavy metal stress. Plant Biol. *16*, 88–96. https://doi.org/10.1111/plb.12017.
66. Bellasio, C., and Griffiths, H. (2014). Acclimation of C4 metabolism to low light in mature maize leaves could limit energetic losses during progressive shading in a crop canopy. J. Exp. Bot. *65*, 3725–3736. https://doi.org/10.1093/jxb/eru052.
67. Doncheva, S., Stoyanova, Z., Georgieva, K., Nedeva, D., Dikova, R., Zehirov, G., and Nikolova, A. (2006). Exogenous succinate increases resistance of maize plants to copper stress. J. Plant Nutr. Soil Sci. *169*, 247–254. https://doi.org/10.1002/jpln.200520560.
68. Bollard, E.G. (1960). Transport in the Xylem. Annu. Rev. Plant Physiol. *11*, 141–166. https://doi.org/10.1146/annurev.pp.11.060160.001041.
69. Ohshima, T., Hayashi, H., and Chino, M. (1990). Collection and Chemical Composition of Pure Phloem Sap from Zea mays L. Plant Cell Physiol. *31*, 735–737. https://doi.org/10.1093/oxfordjournals.pcp.a077972.
70. Gaume, A., Mächler, F., De León, C., Narro, L., and Frossard, E. (2001). Low-P tolerance by maize (Zea mays L.) genotypes: Significance of root growth, and organic acids and acid phosphatase root exudation. Plant Soil *228*, 253–264. https://doi.org/10.1023/A:1004824019289.
71. Lalonde, S., Wipf, D., and Frommer, W.B. (2004). Transport mechanisms for organic forms of carbon and nitrogen between source and sink. Annu. Rev. Plant Biol. *55*, 341–372. https://doi.org/10.1146/annurev.arplant.55.031903.141758.
72. Turgeon, R., and Wolf, S. (2009). Phloem Transport: Cellular Pathways and Molecular Trafficking. Annu. Rev. Plant Biol. *60*, 207–221. https://doi.org/10.1146/annurev.arplant.043008.092045.
73. Ohno, T., Koyama, H., and Hara, T. (2003). Characterization of Citrate Transport through the Plasma Membrane in a Carrot Mutant Cell Line with Enhanced Citrate Excretion. Plant Cell Physiol. *44*, 156–162. https://doi.org/10.1093/pcp/pcg025.
74. Jeong, J., Suh, S., Guan, C., Tsay, Y.-F., Moran, N., Oh, C.J., An, C.S., Demchenko, K.N., Pawlowski, K., and Lee, Y. (2004). A Nodule-Specific Dicarboxylate Transporter from Alder Is a Member of the Peptide Transporter Family. Plant Physiol. *134*, 969–978. https://doi.org/10.1104/pp.103.032102.
75. Lee, M., Choi, Y., Burla, B., Kim, Y.-Y., Jeon, B., Maeshima, M., Yoo, J.-Y., Martinoia, E., and Lee, Y. (2008). The ABC transporter AtABCB14 is a malate importer and modulates stomatal response to CO2. Nat. Cell Biol. *10*, 1217–1223. https://doi.org/10.1038/ncb1782.
76. Girke, C., Daumann, M., Niopek-Witz, S., and Möhlmann, T. (2014). Nucleobase and nucleoside transport and integration into plant metabolism. Front. Plant Sci. *5*, 443.
77. Satish Kumar, V., Dasika, M.S., and Maranas, C.D. (2007). Optimization based automated curation of metabolic reconstructions. BMC Bioinf. *8*, 212–216. https://doi.org/10.1186/1471-2105-8-212.
78. Caemmerer, S. (2000). Biochemical Models of Leaf Photosynthesis. https://doi.org/10.1071/9780643103405.
79. Wittig, U., Kania, R., Golebiewski, M., Rey, M., Shi, L., Jong, L., Algaa, E., Weidemann, A., Sauer-Danzwith, H., Mir, S., et al. (2012). SABIO-RK—database for biochemical reaction kinetics. Nucleic Acids Res. *40*, D790–D796. https://doi.org/10.1093/nar/gkr1046.
80. Chowdhury, R., Bouatta, N., Biswas, S., Floristean, C., Kharkar, A., Roy, K., Rochereau, C., Ahdritz, G., Zhang, J., Church, G.M., et al. (2022). Single-sequence protein structure prediction using a language model and deep learning. Nat. Biotechnol. *40*, 1617–1623. https://doi.org/10.1038/s41587-022-01432-w.
81. Zardecki, C., Dutta, S., Goodsell, D.S., Voigt, M., and Burley, S.K. (2016). RCSB Protein Data Bank: A Resource for Chemical, Biochemical, and Structural Explorations of Large and Small Biomolecules. J. Chem. Educ. *93*, 569–575. https://doi.org/10.1021/acs.jchemed.5b00404.
82. Berman, H.M. (2008). The Protein Data Bank: a historical perspective. Acta Crystallogr. A *64*, 88–95. https://doi.org/10.1107/S0108767307035623.
83. Zhang, Y., and Skolnick, J. (2005). TM-align: a protein structure alignment algorithm based on the TM-score. Nucleic Acids Res. *33*, 2302–2309. https://doi.org/10.1093/nar/gki524.
84. Kopylova, E., Noé, L., and Touzet, H. (2012). SortMeRNA: fast and accurate filtering of ribosomal RNAs in metatranscriptomic data. Bioinformatics *28*, 3211–3217. https://doi.org/10.1093/bioinformatics/bts611.
85. Bushnell, B. (2014). BBMap: A Fast, Accurate, Splice-Aware Aligner (Lawrence Berkeley National Lab. (LBNL)).
86. Dobin, A., Davis, C.A., Schlesinger, F., Drenkow, J., Zaleski, C., Jha, S., Batut, P., Chaisson, M., and Gingeras, T.R. (2013). STAR: ultrafast universal RNA-seq aligner. Bioinformatics *29*, 15–21. https://doi.org/10.1093/bioinformatics/bts635.
87. Lambert, I., Paysant-Le Roux, C., Colella, S., and Martin-Magniette, M.-L. (2020). DiCoExpress: a tool to process multifactorial

RNAseq experiments from quality controls to co-expression analysis through differential analysis based on contrasts inside GLM models. Plant Methods *16*, 68. https://doi.org/10.1186/s13007-020-00611-7.

88. Baudry, K., Roux, C.P.-L., Colella, S., Castandet, B., and Martin, M.-L. (2022). Analyzing Multifactorial RNA-Seq Experiments with DiCoExpress. JoVE *185*, e62566. https://doi.org/10.3791/62566.
89. Robinson, M.D., McCarthy, D.J., and Smyth, G.K. (2010). edgeR: a Bioconductor package for differential expression analysis of digital gene expression data. Bioinformatics *26*, 139–140. https://doi.org/10.1093/bioinformatics/btp616.
90. McCarthy, D.J., Chen, Y., and Smyth, G.K. (2012). Differential expression analysis of multifactor RNA-Seq experiments with respect to biological variation. Nucleic Acids Res. *40*, 4288–4297. https://doi.org/10.1093/nar/gks042.
91. Rigaill, G., Balzergue, S., Brunaud, V., Blondet, E., Rau, A., Rogier, O., Caius, J., Maugis-Rabusseau, C., Soubigou-Taconnat, L., Aubourg, S., et al. (2018). Synthetic data sets for the identification of key ingredients for RNA-seq differential analysis. Brief. Bioinform. *19*, 65–76. https://doi.org/10.1093/bib/bbw092.

STAR★METHODS

KEY RESOURCES TABLE

REAGENT or RESOURCE	SOURCE	IDENTIFIER
Deposited data		
iZMA6517, EXTREAM, and MBA	Chowdhury et al.[19](this work)	https://github.com/ssbio/iZMA6517
Structure Informed Turnover rate	Chowdhury et al.[19](this work)	https://github.com/ChowdhuryRatul/kcat_iZMA6517
Deep Learning-based Turnover	Li et al.[51]	https://www.nature.com/articles/s41929-022-00798-z
K-mean clustering	Ahmed and Dey, 2007	https://doi.org/10.1016/j.datak.2007.03.016
Min/Max driving force analysis	Noor el al.[33]	PMC3930492
E-flux	Coljin et al.	PMC2726785
GAMS	GAMS	https://www.gams.com/
CPLEX solver	IBM	https://www.ibm.com/products/ilog-cplex-optimization-studio/cplex-optimizer
Temperature stress transcriptomics data	Makarevitch et al.[22]	PMC4287451
NaCl	VWR Chemicals	27788.366
$Ca(NO_3)_2,4H_2O$	VWR Chemicals	22384.367
$CaCl_2,2H_2O$	VWR Chemicals	22322.364
$Mg(SO_4),7H_2O$	VWR Chemicals	25163.364
KNO_3	Sigma-Aldrich	49143
KCl	VWR Chemicals	26752.366
KH_2PO_4	VWR Chemicals	26923.367
K_2SO_4	VWR Chemicals	26994.362
$(NH4)_6Mo_7O_{24}$	Sigma-Aldrich	431346
H_3BO_3	VWR Chemicals	20185.260
$MnSO_4$	VWR Chemicals	25303.233
$ZnSO_4$	VWR Chemicals	29253.236
Sequestrene 138 FE 100	Syngenta	30643
TRIzol® Reagent	Ambion	15596026
RNA Clean & Concentrator-5 w/Zymo-Spin IC Columns	OZYME	ZR016
1 kb Plus DNA Ladder	Invitrogen	10787026
Dnase I,Rnase-free	Thermo Scientific	EN0531
dNTP Mix 25 mM each	Thermo Scientific	R1122
RiboLock RNase Inhibitor	Thermo Scientific	EO0382
RevertAid H Minus Reverse Transcriptase (200 U/μL)	Thermo Scientific	EP0452
Takyon™ ROX SYBR 2X Mastermix dTTP	Eurogentec	UF-RSMT-B0701
Fragment Analyzer RNA Kit	AGILENT	DNF-471-0500
Fragment Analyzer DNA Kits	AGILENT	DNF-477-0500
Bioanalyzer RNA Nano 6000 kit	AGILENT	5067–1511
Quant-iT™ RiboGreen	Thermo Scientific	R-11491
0.5–10 Kb RNA Ladder	Thermo Scientific	AM7150
1 kb DNA Ladder	New England Biolabs	N3232L
Quant-iT™ PicoGreen™ dsDNA Reagent	Thermo Scientific	P7581
Illumina® Stranded mRNA Prep, Ligation (96 samples)	ILLUMINA	20040534

(*Continued on next page*)

Continued

REAGENT or RESOURCE	SOURCE	IDENTIFIER
IDT for Illumina RNA UD Indexes Set A (96 indexes, 96 samples)	ILLUMINA	20040553
AMPURE XP SPRI REAGENT 60 ML	BECKMAN COULTER	A63881
Agencourt RNA clean XP	BECKMAN COULTER	A63987
Ethanol absolute for BM 500 ML	Sigma-Aldrich	51976-500ML-F
NovaSeq 6000 S4 Reagent Kit v1.5 (300 cycles)	ILLUMINA	20028312
Phi X Control V3	ILLUMINA	FC-110-3001
R	R Studio	V 4.0.567
CATdb	Complete Arabidopsis Transcriptome database	V 1.0
RNA-seq Data	Gene Expression Omnibus	GSE235654

RESOURCE AVAILABILITY

Lead contact

Further information and requests for resources should be directed to and will be fulfilled by the lead contact, Dr. Rajib Saha (rsaha2@unl.edu).

Materials availability

The study did not generate new materials.

Data and code availability

- *i*ZMA6517, EXTREAM, and MBA codes are publicly available in this GitHub directory: https://github.com/ssbio/iZMA6517. SI-k_{cat} codes are available in this GitHub directory: https://github.com/ChowdhuryRatul/kcat_iZMA6517. RNAseq project is deposited in Gene Expression Omnibus (GSE235654) and publicly available. All steps of the experiment, from growth conditions to bioinformatic analyses, were detailed in CATdb: http://tools.ips2.u-psud.fr.fr/CATdb/; Project: NGS2021_19_Rhizophagus according to the MINSEQE. Nutrients for the plant growth can be accessed in Table S13.
- All statistical analyses were run in R 4.0.567 using code that implement the algorithms described in the papers that introduced these statistical tests.[33,59] All scripts are available upon request.
- The lead contact will provide any additional information needed to reanalyze the data reported in the paper.

EXPERIMENTAL MODEL AND SUBJECT DETAILS

Plant experiments

The maize line used in this study is B73. The fungal strain used is the highest quality of purity strain *Rhizophagus irregularis* DAOM197198 (Agronutrition Montpellier France). In all experiments, maize seeds were surface-sterilized as follows. Seeds were first incubated in ethanol for 5 min at 28°C followed by rinsing with distilled water. Then the seeds were incubated for 45 min in a 15% commercial bleach solution with 0.01% Triton x100 then rinsed in distilled water. They were placed on wet sterile Watman paper in Petri dishes closed with parafilm and incubated in the dark for 48-72 h at 20°C. Germinated seeds were selected and then sown in the experimental setup.

METHOD DETAILS

K-means clustering analysis

K-means clustering[60] algorithm was used to classify different genes into different clusters. Number of clusters was determined using the Elbow method. The whole K-mean clustering was implemented in Python, using numpy, pandas, and sklearn modules. Default setting of K-mean clustering, mentioned in the sklearn, was not changed in this study. Number of clusters were determined using the elbow method (Figure S24). The elbow method is a graphical approach to determining the best number of clusters (K) value in the K-means clustering algorithm. The elbow graph depicts the within-cluster sum-of-square values on the y axis for various K values. The ideal K value is the point on the graph when it forms an elbow. To perform the K-mean clustering, we used 4 clusters, 10 centroid seeds, 300 maximum iteration, and 10^{-4} relative tolerance.

Genome-scale metabolic model reconstruction

Determining the primary set of reactions for stalk and kernel tissue

A previously published leaf genome-scale model[27] was used as a scaffolding to reconstruct the stalk and kernel tissues. Microarray data[61] was used to determine the set of metabolic genes that were categorized as highly or lowly expressed in each tissue based on the gene's maximum expression level in the measured growth stages and tissues. Genes with an expression level above the cut-off (7.644) were categorized as "highly expressed." "Lowly expressed" genes were defined as genes with an expression level below the cut-off in all growth stages for the focus tissue, but have a measured expression level above the cut-off in at least one other tissue. Finally, genes that were expressed at a level that is always below the cut-off for all growth stages and tissues were categorized as "always-lowly expressed." Genes contained within the model GPR relationships that were not included in the microarray data were included in the "always lowly expressed" set. Therefore, the "always lowly expressed" set includes all genes with no conclusive evidence. Within the model, GPR relationships are defined using Boolean logic with isozymes represented by an "OR" relationship and subunits represented by an "AND" relationship. To determine the primary set of reactions for each tissue-specific model, genes in the "highly expressed" set were assigned "True" in the Boolean logic and genes in the "lowly expressed" set were assigned "False." Genes in the "always lowly expressed" set that are associated with a gene categorized into either of the two other tissue specific sets were assumed to be co-expressed with their measured isozymes or subunits. In this way, "always lowly expressed" genes cannot determine a reaction's presence in the tissue-specific model. For example, a gene in the "always lowly expressed" set that is associated with a "False" isozyme or subunit (i.e., a gene in the "tissue lowly expressed" set) will be defined as "False" in the GPR Boolean logic relationship. This categorization based on co-expression was completed manually for 14 of the 2109 unique reactions (i.e., the full set of metabolic reactions independent of the compartment or tissue). Reactions with GPR relationships that only contain genes in the "always lowly expressed" set were placed in the set of not measured reactions. Reactions that were categorized as present based on their GPR relationship are referred to as the primary set of reactions for that tissue. While reactions that were categorized as absent based on their GPR relationship are referred to as the inactive set of reactions.

Creating stalk and kernel biomass reactions and ATP maintenance

Tissue-specific biomass reactions were created based on reported literature values. Each tissue-specific biomass reaction was normalized so that the molecular weight of all biomass components sums to 1 g $mmol^{-1}$ to ensure that there is no bias based on the proportion of biomass components included for each tissue.[62] This normalization is especially important as multiple tissues are growing simultaneously to ensure growth is not artificially favored toward tissues with low biomass weights. Growth and non-growth associated ATPM levels were based on leaf measurements[59,63–65] for photosynthetic tissues and on root measurements[64,66,67] for non-photosynthetic tissues.

Vascular tissue transport

The metabolites that are transported through the phloem and xylem tissues,[68–72] as well as the transport costs predicted for each metabolite,[71,73–76] were identified based on the literature. The phloem and xylem tissues were combined together for simplicity in the model and are referred to as vascular tissue.

Creating stalk and kernel models

The primary set of reactions $J_{Primary}$, vascular tissue transporters Vt and environmental nutrients $J_{Nutrients}$ supplied to stalk and kernel were combined to form the draft model for each tissue. When modeling stalk and kernel models, the nutrients include both those from environment, but also include those metabolites that can be imported from the vascular tissue. Inactive reactions, determined by using the microarray data and GPR relationships, were placed into a set termed $J_{Inactive}$, which is unique for each tissue. Finally, spontaneous reactions and reactions with a GPR relationship that only contain genes in the "always lowly expressed" set were placed into the set $J_{NotMeasured}$, which is by definition equivalent for each tissue. In order to ensure that each tissue-specific biomass reaction was not blocked given the available nutrients to the tissue, (i.e., metabolites imported by the vascular tissue and the environment), a GapFill step[77] was performed for each tissue individually. The following algorithm was used to determine the minimum number of reactions added with a preference of adding reactions from the not measured set over reactions in the inactive set:

$$\text{minimize} \sum_{j \in J_{NotMeasured}} y_j + 10 \sum_{j \in J_{Inactive}} y_j$$

s.t.

$$\sum_{j \in J} S_{ij} v_j = 0, \forall i \in I \quad \text{(Equation 1)}$$

$$LB_j \leq v_j \leq UB_j, \forall j \in J_{Primary} \cup J_{Nutrients} \cup Vt \quad \text{(Equation 2)}$$

$$LB_j y_j \leq v_j \leq UB_j y_j, \forall j \in J_{Inactive} \cup J_{NotMeasured} \quad \text{(Equation 3)}$$

$$v_{biomass} \geq 0.001 \quad \text{(Equation 4)}$$

Here S_{ij} is the stoichiometric coefficient of metabolite i in reaction j and v_j is the flux through reaction j. I and J are sets that include all metabolites and reactions known to occur within maize, respectively. The pseudo-steady state assumption (1) assumes that the tissue is growing efficiently, and all internal metabolites are produced and consumed at an equal rate. The lower bound, LB_j, and upper bound, UB_j, of reaction j (2 and 3) are sufficiently small and large and are determined by each reaction's directionality based on thermodynamic constraints. The binary variable, y_j, is equal to 1 if the reaction is added to the model and 0 otherwise (3). Finally, a small amount of flux is forced through the biomass Equation 4 to ensure biomass is not blocked. From this algorithm, a set of reactions, $J_{Secondary}$, was added to the draft tissue-specific models to ensure flux through the biomass reaction is possible.

A second GapFill step was completed to activate as many reactions in the primary set as possible for stalk and kernel. The GapFill algorithm displayed above was completed successively for each reaction that did not carry flux in the primary set by modifying the model constraints in the following manner. First, (2) was extended to encompass the secondary set of reactions to account for their inclusion in the tissue-specific model. Second, (4) was applied to the reaction of interest rather than the biomass reaction. Reactions from the not measured set were added as needed, however reactions from the inactive set were only included in the final model if their addition allowed ten previously blocked reactions from the active set carry flux. This was done to ensure that reactions with genes that are lowly expressed in the tissue based on transcriptomic data were added only if they allow for flux through multiple reactions in the primary set. The final set of reactions included in stalk and kernel was defined for each tissue k as J_k.

Incorporating additional constraints based on literature evidence

To accurately capture the efficiency of photosynthesis, it is pertinent to understand the relationship between rubisco carboxylase and oxygenase. The maximum rate of carboxylation and oxygenation are related by the following equation:

$$\frac{V_c}{V_o} = \frac{k_o}{k_c S_R} \quad \text{(Equation 5)}$$

Here, The Michaelis-Menten constants for oxygenation (k_o) and carboxylation (k_c) and the rubisco specific S_R were set to values typical of C4 species,[78] $k_c = 650 \mu molmol^{-1}$, $k_c = 450 \mu molmol^{-1}$, $S_R = 2590$. Equation 5 works indicates the maximum possible rate of carboxylation an oxygenation and thus set in the model simulation:

EXpression disTributed REAction flux Measurement algorithm

In this work, we proposed the EXTREAM, where transcript of each gene was equally divided based on the number of reactions the gene participated. We also changed the objective function which is the minimization of sum of reaction fluxes compared to a reference condition, calculated from the transcriptomics data.

The formulation of EXTREAM is the following:

$$min \sum_j \left(|v_j| - v_{j,omics} \right)$$

Subject to,

$$\sum_j S_{i,j} v_j = 0, \forall i \in I \quad \text{(Equation 6)}$$

$$v_{j,min} \leq v_j \leq v_{j,max}, \forall j \in J \quad \text{(Equation 7)}$$

$$v_{biomass} \leq f \times v_{biomass,max} \quad \text{(Equation 8)}$$

Here, v_j is the flux to be calculated for reaction J, $v_{j,omics}$ is the reference condition calculated from the GPR association for reaction J, $S_{i,j}$ is the stoichiometric matrix for metabolite I, and reaction J, $v_{j,min}$ and $v_{j,max}$ are the upped and lower bound of reaction J, $v_{biomass}$ is the desired biomass growth rate, $v_{biomass,max}$ is the maximum possible biomass growth rate, and f is fraction between 0 and 1. To reformulate the EXTREAM algorithm to a linear optimization problem and will also introduce the transcript distribution to better constraint the solution space.

Let's assume two genes has the following expressions:

$G_1 = 10$

$G_2 = 20$

And there are three reactions associated with G_1 and G_2 as following

$R_1 = G_1$ or G_2

$R_2 = G_1$

$R_3 = G_2$

Then according to the E-flux algorithm, v_j can be calculated as following:

R_1 = 30 mmol/gDW/hr

R_2 = 10 mmol/gDW/hr

R_3 = 20 mmol/gDW/hr

If R_1 is a forward reaction then the bounds on reaction will be $0 \leq R_1 \leq 30$. Similarly, if R_1 is a forward reaction then the bounds on reaction will be $-30 \leq R_1 \leq 30$. Same will be true for other reactions, such as R_2 and R_3.

According to the EXTREAM algorithm, the transcript will be distributed equally based on the number of reactions a gene participates. Furthermore, the reference condition. $v_{j,omics}$, can be calculated as following:

R_1 = 15 mmol/gDW/hr

R_2 = 5 mmol/gDW/hr

R_3 = 10 mmol/gDW/hr

From EXTREAM, if R_1 is a forward reaction then the bounds on reaction will be $0 \leq R_1 \leq 15$. Similarly, if R_1 is a forward reaction then the bounds on reaction will be $-15 \leq R_1 \leq 15$. Same will be true for other reactions, such as R_2 and R_3. Thus, EXTREAM algorithm provides a tighter bounds on reaction fluxes compared to the E-flux algorithm and can be useful for realistic phenotypical predictions.

As the original formulation is a non-smooth optimization problem, the linearization of such non-smooth optimization problem can be achieved as the following:

$$min \sum_j \left(v_{j,new} - v_{j,omics}\right)$$

Subject to,

$$\sum_j S_{i,j} v_j = 0, \forall i \in I \quad \text{(Equation 9)}$$

$$v_j \leq v_{j,new} + v_{j,omics}, \forall j \in J \quad \text{(Equation 10)}$$

$$-v_j \leq v_{j,new} - v_{j,omics}, \forall j \in J \quad \text{(Equation 11)}$$

$$v_{j,min} \leq v_j \leq v_{j,max}, \forall j \in J \quad \text{(Equation 12)}$$

$$v_{biomass} \leq f \times v_{biomass,max} \quad \text{(Equation 13)}$$

Here, $v_{j,new}$ is a replacement variable used in the reformulation.

MBA

To determine the metabolic bottleneck in a GSM, we proposed the following algorithm.

$$\begin{bmatrix} Max\ v_{biomass} \\ Subject to: \\ \sum_{j=1}^{m} S_{ij} v_j = 0, i \in I\ (14) \\ a_j \leq v_j \leq b_j, j/\{j'\} \in J\ (15) \\ v_{j',\min,} \leq v_{j'} \leq v_{j',\max}, j' \in J (16) \end{bmatrix}, \forall j' \in J$$

Here a_j is the lower bound reaction v_j and b_j is the upper bound of reaction v_j. Both a_j and b_j were calculated from the transcriptomics data and GPR association. $v_{j',min}$ is the expanded lower bound of the reaction j' and $v_{j',max}$ is the expanded upper bound of the reaction j'. In this case, we set $v_{j',min} = -1000 \frac{mmol}{gDW.hr}$ and $v_{j',max} = 1000 \frac{mmol}{gDW.hr}$. We solved the optimization problem by maximizing the biomass $v_{biomass}$ for the new expanded flux space of each reaction j' in an iterative manner and then recorded the biomass growth rate. From this biomass growth rate collections, we can check for which j' biomass growth rate increased. Then that j' can be considered as the metabolic bottleneck of a given metabolic network.

Min/Max Driving Force analysis

To find out the thermodynamic driving force and thermodynamic bottleneck of a given pathway, we used max/min driving force analysis (MDF) from the literature.[33] In this method, we maximized the driving force of each reaction in a given pathway within the biologically relevant concentration and found the maximum possible driving force of a pathway. The formulation of MDF analysis is given below:

$$\max B$$

Subject to:

$$-\Delta G \geq B \quad \text{(Equation 14)}$$

$$\Delta G = \left(\Delta G^0 + RT \cdot S^T \cdot x\right) \quad \text{(Equation 15)}$$

$$\ln(C_{\min}) \leq x \leq \ln(C_{\max}) \quad \text{(Equation 16)}$$

ΔG^0 is the standard Gibbs free energy, R is the gas constant, T (5^0 C for cold stress and 50^0 C for heat stress) is the temperature, and x *and* C indicates concentration. This analysis is particularly useful when metabolomics information is not fully available for a given pathway. Thus biologically relevant metabolite concentration range can be used to infer information about a pathway, whether it will be thermodynamically feasible or not. Furthermore, we fixed the ATP/ADP and NADH/NAD ratio as mentioned in the original MDF article, $\frac{[ATP]}{[ADP]} = 10$ and $\frac{[NADH]}{[NAD^+]} = 0.1$.[33] We simulated the MDF problem for different concentrations of target metabolites, mostly cofactors such as ATP and NAD^+ and recorded the change in MDF values.

Structure informed k_{cat} prediction (SI-k_{cat})

The sequential protocol followed for k_{cat} prediction is as follows:

Database scraping for k_{cat} values

The SABIO-RK[79] database was scraped for k_{cat} values using E.C Number, KEGG reaction ID, and KEGG Compound IDs as search query. The obtained k_{cat} values are refined using source organism (*Zea mays*). In cases where no k_{cat} values are reported for *Zea mays*, other phylogenetically close organisms are considered.

Structure modeling of enzymes from protein sequence

Geometric deep learning-based, single sequence protein structure predictor (RGN2) is employed to model the 3D atomic coordinates of enzyme in PDB format.[80]

Tertiary structure collection of experimentally resolved enzymes

The experimentally resolved 3D structure of enzymes belonging to the same EC number and preferably same organism (Zea mays) are collected from RCSB Protein DataBank (https://www.rcsb.org/).[81,82]

Structural similarity weightage (Sw) calculation

The 3D structures of the enzymes modeled in step (b) and the experimentally resolved enzymes (c) are aligned to estimate the similarities/differences between their structures. Distance root mean square distance (dRMSD) between consecutive atom pairs are calculated and averaged over the total number of pairs to give TM-score (Template Modeling score). This is done using TM-align web server (https://zhanggroup.org/TM-align/).[83] TM-score ranges from 0 to 1, where 0 indicates no similarity in structure, while 1 indicates 100% structural similarity.

Structure Informed k_{cat} prediction ($SI - k_{cat}$)

The k_{cat} prediction follows the following weighted averaging function:

$$SIk_{cat} = \frac{S_{wa}.k_{cat\ a} + S_{wb}.k_{cat\ b} + \ldots S_{wn}k_{cat\ n}}{S_{wa} + S_{wb} + \ldots S_{wn}} \quad \text{(Equation 17)}$$

Where Sw refers to structural similarity weightage (TM-score) between modeled and experimentally reported structures and k_{cat} refers to k_{cat} values scraped from SABIO-RK for the corresponding reaction and enzyme class.

Error estimation of structure-informed k_{cat} values ($SI - k_{cat}$)

The standard deviation of predicted k_{cat} values were calculated from the protein sequence dissimilarity index. It is to be noted that similar structural motifs in proteins did not necessarily mean identical protein sequences. Moreover, enzyme kinetics is dependent on the presence of specific amino acids and the structural motifs that hold them together. Therefore, pairwise protein sequence alignment is carried out between structures from step (b) and step (c) as an estimate of standard deviation of $SI - k_{cat}$.

Validation of structure-informed k_{cat} values ($SI - k_{cat}$)

The k_{cat} predicted by the $SI - k_{cat}$ algorithm matched reasonably well with the experimental predictions (Figures S17–S21). Comparison is provided between this method and other computational algorithm as well.[51]

Once the k_{cat} is determined, the following equation[50] was used to determine the relationship between enzyme concentration (E) and saturation (K):

$$E = \frac{v_{reaction}}{k_{cat}.\left(1 - e^{\frac{\Delta G}{RT}}\right)} \times \frac{1}{K} \quad \text{(Equation 18)}$$

Here, ΔG values were collected from the corresponding MDF analysis, and $v_{reaction}$ were collected by solving contextualized *i*ZMA6517 for heat and/or cold stress.

R. irregularis symbiosis of maize root

Plant material, growth conditions and inoculation

The experimental design and the different steps of growing and harvesting for RNAseq experiment, performed in 2020, are indicated in Figure S25. Briefly, germinated seeds were sown in pots of 4 L containing a mix of sterilized unfertilized peat and dried clay beads (1:1/v/v). A first inoculation was performed with 500 spores of *R. irregularis*, a second inoculation was performed 1 week after sowing with 200 spore/plant, and a third inoculation was performed 2 weeks after sowing with 200 spore per plant. Control plants were treated with distilled water. Plants were grown under three different nitrogen regimes (1 mM NO_3^- herein named LN, medium N 5 mM NO_3^- and high N (HN) 10 mM NO_3^-). Details for nutrient solution composition are given in Table S13. For each N regime, plants were irrigated for the first three weeks with the solution corresponding to the chosen N regime with low P (named P-) containing 10 μM Phosphate in order to trigger AMF colonization. Then, at the indicated date in Figure S25, irrigation was turned into the same N level but containing 300 μM P. Increasing P level in the irrigation solution was necessary to allow plants reach the maturity stage.

Harvesting procedures

For RNA extractions, leaf and root samples were harvested and frozen in liquid nitrogen before extraction. The harvesting stage corresponds to 15 days after tasseling which has been shown to provide a good indication of root colonization (data not shown). Dates of harvesting differed depending on the condition (Figure S25). A piece of 1 cm × 10 cm leaf surface from the leaf below the ear of each individual plant was harvested. Thin secondary roots were harvested from the surrounding root system, close to the pot borders. They were washed with distilled water and then frozen in liquid nitrogen.

RNA extraction for RNAseq

RNA extraction was performed with an adapted TRIZOL (TRIZOL by Invitrogen – Thermo Fisher Products & Kits) protocol followed by purification on Zymo-Spin column. Fresh tissue of leaves or roots (100 mg) were frozen in liquid nitrogen then ground to fine powder that was homogenized in 1 mL of TRIZOL. Two glass beads were added to the extract in the tube and vortexed for 5 min, then incubated for 5 min at room temperature (RT). Two hundred microliters of chloroform were added, then the sample was vortexed for 5 min and incubated for 3 min at RT. Samples were centrifuged at 12,000g for 15 min at 4°C. The aqueous phase (approximately 500 μL) was transferred to a new tube where an equal volume of ethanol (95–100%) was added. The sample mixed with ethanol was then transferred to a Zymo-Spin IC column and purification was proceeded following manufacturer instructions.

RNAseq and bioinformatic analysis

RNA-seq libraries were constructed by the POPS platform (IPS2) using the Illumina Stranded mRNA Prep kit (Illumina, California, U.S.A.) according to the supplier's instructions. Libraries were sequenced by the Genoscope on a Novaseq 6000 instrument (Illumina) with 150 base paired-end sequences.

Raw data cleaning

The raw data were first cleaned by the Genoscope as follows.

Illumina filter. To remove the least reliable data from the analysis, the raw data were filtered to remove any clusters that have "too much" intensity corresponding to bases other than the called base. The purity of the signal from each cluster was examined over the first 25 cycles and calculated as Chastity = Highest_Intensity/(Highest_Intensity + Next_Highest_Intensity) for each cycle. The default filtering implemented at the base calling stage allows at most one cycle that is less than the Chastity threshold (0,6).

Genoscope filter. We remove adapters and primers on the whole read and low-quality nucleotides from both ends (while quality value is lower than 20) and then continue next steps with the longest sequence without adapters and low quality bases. Then we removed sequences between the second unknown nucleotide (N) and the end of the read. This step is done on trimmed (adapters + quality) reads. We then discard reads shorter than 30 nucleotides after trimming. Later we removed read pairs that come from the low-concentration spike-in library of Illumina PhiX Control. Next, reads pairs corresponding to ribosomal RNA were removed using sortMeRNA (v2.1[84]). We cleaned reads from

Genoscope were adapter-trimmed again by the POPS platform with BBduk from the BBmap suite (v38.84)[85] with the options k = 23 ktrim = r qtrim = r useshortkmers = t mink = 11 trimq = 20 hdist = 1 tpe tbo minlen = 30 using adapter sequences file included in the BBTools package.

Mapping and gene expression quantification. Filtered reads were then mapped and counted using STAR (v2.7.3a[86]) with the following parameters –alignIntronMin 5 –alignIntronMax 60000 –outSAMprimaryFlag AllBestScore –outFilterMultimapScoreRange 0 –outFilterMultimapNmax 20 on a combined reference genome made by concatenating the files of the *Zea mays* B73 (V4.49) reference genome and the associated GTF annotation files (also combined). Between 73.26 and 96.13% of the reads were uniquely mapped (median = 94.80%). Between 73.84 and 87.99% of the reads were associated with annotated genes (median = 87.28%).

Software and hardware resources

The General Algebraic Modeling System (GAMS) version 24.7.4 was used to run EXTREAM, MBA, and the OptFill algorithm on the model. GAMS was run on a high-performance cluster computing system at the Holland Computing Center of the University of Nebraska-Lincoln. The K-mean clustering was implemented in Python, using numpy, pandas, and sklearn modules. Transcriptomics data analysis was performed in R module.

QUANTIFICATION AND STATISTICAL ANALYSIS

Statistical analyses were conducted on R v3.6.2 (R Core Team, 2020) using the script-based tool DiCoExpress.[87,88] DiCoexpress used the Bioconductor package edgeR (v 3.28.0,.[89,90] The raw count file used for the statistical analyses only contain the reads of the *Zea mays* organism. Dicoexpress analyzes RNAseq projects with at most two biological factors. For this reason and to answer biological questions of interest, 4 separate statistical analyses were conducted on samples from leaves and roots.

Gene filtering and normalization

For the four analyses, low counts genes were filtered using the "FilterByExpression" feature available through the edgeR package with a minimum count threshold of 15. Raw counts were normalized with the trimmed mean of M values (TMM) method implemented in edgeR package.

Differential Expression analysis

The differential analysis is based on a negative binomial generalized linear model. For the 4 *Zea mays* analyses, the log2 of the average normalized gene expression is an additive function of a treatment effect (inoculation or control), an interaction between the condition and the treatment and the technical replicate factor (3 modalities for each nutritional condition LN and HN). To make the processing of these multifactorial designs easier, Differential Expression (DE) analyses were performed using the DiffAnalysis_edgeR function of DiCoExpress to automatically generate the contrasts. In each analysis, we considered the difference between the two treatment modalities and averaged on the two condition modalities LN and HN). For each contrast a likelihood ratio test was applied, and raw p values were adjusted with the Benjamini–Hochberg procedure to control the false discovery rate. The distribution of the resulting p values followed the quality criterion described by Rigaill et al.[91] A gene was declared differentially expressed if its adjusted p value is lower than 0.05.